Early Spring Phytoplankton Dynamics in the Western Antarctic Peninsula

Correspondence to:
K. R. Arrigo,
arrigo@stanford.edu

Kevin R. Arrigo[1] [iD], **Gert L. van Dijken[1]** [iD], **Anne-Carlijn Alderkamp[1,2]**, **Zachary K. Erickson[3]** [iD], **Kate M. Lewis[1]**, **Kate E. Lowry[1]** [iD], **Hannah L. Joy-Warren[1]**, **Rob Middag[4,5]** [iD], **Janice E. Nash-Arrigo[6]**, **Virginia Selz[1]** [iD], **and Willem van de Poll[7]** [iD]

[1]Department of Earth System Science, Stanford University, Stanford, CA, USA, [2]Now at Department of Biological and Health Sciences, Foothill College, Los Altos Hills, CA, USA, [3]Division of Geological and Planetary Sciences, California Institute of Technology, Pasadena, CA, USA, [4]Department of Ocean Systems, NIOZ Royal Netherlands Institute for Sea Research, and Utrecht University, Texel, The Netherlands, [5]Department of Chemistry, NIWA/University of Otago Research Centre for Oceanography, Dunedin, New Zealand, [6]Palo Alto Unified Schools, Palo Alto, CA, USA, [7]Department of Ocean Ecosystems, Energy and Sustainability Research Institute Groningen, University of Groningen, Groningen, The Netherlands

Abstract The Palmer Long-Term Ecological Research program has sampled waters of the western Antarctic Peninsula (wAP) annually each summer since 1990. However, information about the wAP prior to the peak of the phytoplankton bloom in January is sparse. Here we present results from a spring process cruise that sampled the wAP in the early stages of phytoplankton bloom development in 2014. Sea ice concentrations were high on the shelf relative to nonshelf waters, especially toward the south. Macronutrients were high and nonlimiting to phytoplankton growth in both shelf and nonshelf waters, while dissolved iron concentrations were high only on the shelf. Phytoplankton were in good physiological condition throughout the wAP, although biomass on the shelf was uniformly low, presumably because of heavy sea ice cover. In contrast, an early stage phytoplankton bloom was observed beneath variable sea ice cover just seaward of the shelf break. Chlorophyll *a* concentrations in the bloom reached 2 mg m^{-3} within a 100–150 km band between the SBACC and SACCF. The location of the bloom appeared to be controlled by a balance between enhanced vertical mixing at the position of the two fronts and increased stratification due to melting sea ice between them. Unlike summer, when diatoms overwhelmingly dominate the phytoplankton population of the wAP, the haptophyte *Phaeocystis antarctica* dominated in spring, although diatoms were common. These results suggest that factors controlling phytoplankton abundance and composition change seasonally and may differentially affect phytoplankton populations as environmental conditions within the wAP region continue to change.

1. Introduction

The waters of the western Antarctic Peninsula (wAP) have been studied extensively, especially since the initiation of the Palmer Station Long-Term Ecological Research (Pal-LTER) program in 1990 (Ducklow et al., 2007). This interest is due in large part to the dramatic increases in temperature that have been recorded in this region in recent decades in both the atmosphere (Turner et al., 2012) and the ocean (Meredith & King, 2005), as well as the corresponding loss of sea ice, particularly in the northern half of the peninsula (Stammerjohn et al., 2012). This area is also of interest because of the biological richness of its coastal ecosystems (Ducklow et al., 2013; Montes-Hugo et al., 2009), supported mainly by the intense growth of phytoplankton in continental shelf waters (<500 m depth) during the summer months (Smith et al., 2008).

Because of its high water column inventory of nutrients, rates of phytoplankton growth and primary production in the wAP are determined primarily by light availability (Vernet et al., 2008). Light levels in the water column at these high latitudes are controlled by a combination of cloud cover, solar zenith angle (seasonal and daily), sea ice and snow cover, and mixed layer depth (MLD). In early austral spring when sun angles are low, mixed layers are deep (>100 m), and sea ice cover is extensive (90–100%), light levels in the upper water column are diminished (<20 μmol photons m^{-2} s^{-1}) and rates of primary production are uniformly low (Saba et al., 2014). Springtime light limitation is most severe following winters with low ice cover,
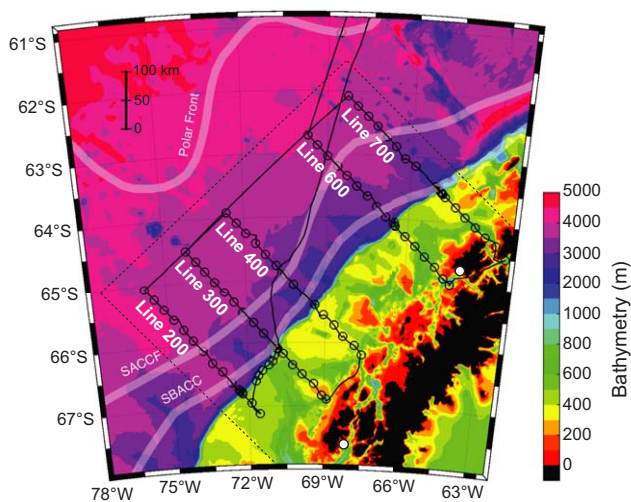
Figure 1. Study area showing bathymetry (colors), ship track (black line), and sampling lines with stations (black circles). Mean locations of the Polar Front, SACCF, and SBACC are as given by Orsi et al. (1995). SACCF, Southern Antarctic Circumpolar Current Front; SBACC, Southern Boundary of the Antarctic Circumpolar Current. Dashed lines denote region from which data from satellite imagery were extracted. White filled circles denote locations of Palmer Station (64.77°S, 64.05°W) and Rothera Station (67.57°S, 68.23°W).

which are characterized by weak stratification and anomalously deep mixed layers (>150 m) resulting from higher exposure to winter winds (Venables et al., 2013).

As solar insolation increases and sea ice melts during austral spring, the mixed layer begins to shoal as a result of thermal and freshwater stratification and phytoplankton growth rates increase, particularly in the marginal ice zone (MIZ). By late spring and summer, sea ice disappears rapidly (~weeks) along much of the wAP. Increased freshwater input from both glacial and sea ice melt increases water column stratification and results in mixed layers that are only 5–10 m deep near the coast and 25–50 m deep on the shelf and slope ~100 km away (Ducklow et al., 2013). Interannual differences in stratification have been shown to impact the intensity of phytoplankton blooms in the vicinity of Rothera Station (Figure 1), with the highest chlorophyll *a* (Chl *a*) concentrations generally following winters of heavy sea ice cover (Ducklow et al., 2013; Rozema et al., 2017). Rates of primary productivity in the wAP peak in January and are highest on the nutrient-rich continental shelf, progressively declining in offshore waters with increasing distance from the coast (Garibotti et al., 2005).

Much of what we know about the factors controlling phytoplankton growth in the wAP comes from the multidecadal time series of cruises that take place each summer as part of the Pal-LTER. Most of these cruises sample the wAP in January or later when the phytoplankton bloom is already at its seasonal peak. Additional information for the region has come from other oceanographic cruises (e.g., RACER; Karl, 1991) and from the more comprehensive seasonal sampling that takes place near Palmer (Kim et al., 2016; Saba et al., 2014) and Rothera Stations (Clarke et al., 2008). However, relatively little is known about the factors that control the large-scale patterns of phytoplankton growth and biomass earlier in the season. Here we present results from an oceanographic research cruise to the wAP during austral spring 2014 when sea ice cover was still quite extensive and phytoplankton biomass was beginning to increase. We characterized the physical and chemical environment over a broad area of the wAP in both ice-covered and ice-free waters and related these characteristics to patterns of phytoplankton growth, abundance, and community composition during this important transition period.

2. Methods

2.1. Study Site

During the second cruise of the research program, Adaptive Responses of *Phaeocystis* Populations in Antarctic Ecosystems (Phantastic II), we collected physical, chemical, and biological data across five hydrographic transects comprising 100 water column stations along the wAP between 31 October and 21 November 2014 (Figure 1) on board the RVIB *Nathaniel B. Palmer*. These transects were chosen to coincide with those sampled later in the season (January–March) during the Pal-LTER program (Smith et al., 1995), although each Phantastic II transect extended an additional 200 km farther seaward than the Pal-LTER grid (200 km; 400 km total). For simplicity, we refer to these transects by their corresponding Pal-LTER line numbers. Regular station spacing was 25 km, although this was reduced to 4 km when crossing the continental shelf break on lines 200, 300, 600, and 700.

2.2. Vertical Profiles

Two conductivity, temperature, and depth (CTD) instruments were used during the cruise: a conventional CTD and a trace-metal clean (TMC) CTD. On 5 November of our cruise, the cable holding the rosette broke and the TMC CTD was lost. Thereafter, we used two spare GO-FLO bottles on a TMC wire to sample for trace metals. Sensors deployed with the conventional CTD-rosette package included a fluorometer (WET Labs ECO-AFL/FL), a transmissometer (WET Labs C-Star), and an oxygen sensor (SBE-43) for all casts, as well as a PAR/Irradiance sensor (Biospherical/Licor) for casts shallower than 1,000 m. Salinity and oxygen measurements were calibrated multiple times per day using an onboard salinometer and amperometric oxygen

titration (Langdon, 2010). Calibrations revealed no significant biases or trends; therefore, measurements were not corrected.

MLD was calculated from vertical profiles as the depth at which density was 0.1 kg m^{-3} greater than at the surface (Dong et al., 2008), although calculated MLD differed little for thresholds ranging from 0.05 to 0.125 kg m^{-3}.

2.3. Discrete Water Samples

Chl a and nutrient concentrations were measured at every station and other filtrations were made only at "full" stations spaced ∼50 km apart (i.e., every other station). Using the conventional CTD rosette, we collected water from standard depths (2, 10, 25, 50, 75, and 100 m). If a fluorescence maximum existed at another depth, then either the closest bottle (if within 10 m) or the 75 m bottle was moved to that depth. Additionally, we collected nutrient samples at the standard depths plus 150, 200, 300, 400, 500, and 750 m using both the conventional CTD and the TMC system described above. At shelf stations with a bottom depth <750 m, we collected seawater from 10 to 20 m above the seafloor.

2.4. Nutrients

Samples for dissolved macronutrient concentrations (nitrate, NO_3^-; nitrite, NO_2^-; phosphate, PO_4^{3-}; and silicate, $Si(OH)_4$) were taken at all stations and depths sampled with the conventional and TMC CTD-rosette package as well as the TMC wire. Samples were collected by filtering seawater through a 0.2 μm syringe filter and stored at $-20°C$ for NO_3^-, NO_2^-, and PO_4^{3-} and at $+4°C$ in the dark for $Si(OH)_4$ to prevent precipitation. Post-cruise nutrient sample analysis took place at the Royal Netherlands Institute for Sea Research (NIOZ) on a WestCo SmartChem 200 discrete autoanalyzer. $NO_3^- + NO_2^-$ is presented as NO_3^- since the contribution of NO_2^- is negligible in Antarctic waters (Kemeny et al., 2016; Serebrennikova & Fanning, 2004).

Dissolved iron (dFe) concentrations were measured directly on board at full stations by the automated Flow Injection Analysis method (Klunder et al., 2011). Filtered and acidified (0.024 M HCl) seawater was concentrated on a column containing aminodiacetid acid (IDA) after inline adjustment to pH 4 using metal-free ammonium acetate buffer. The IDA chelating resin binds only transition metals and not the interfering salts. After washing the column with ultra-pure water, the column was eluted with diluted acid. After mixing with luminol, peroxide and ammonium, the oxidation of luminol with peroxide is catalyzed by Fe and a blue light is produced and detected with a photon counter. The amount of Fe is calculated using a standard calibration line, where a known amount of Fe is added to low Fe-containing seawater. Using this calibration line, the number of counts per nM Fe is obtained. Samples were analyzed in triplicate and standard deviations are given.

The blank was determined daily by analyzing acidified Milli-Q water. Because the blank values were <0.01 nM dFe, no correction was made. The average limit of detection (0.010 ± 0.006 nM dFe) was defined as 3 times the standard deviation of the Sampling and Analysis of Fe (SAFe) S reference sample that was analyzed 4 times during this expedition. At the start of every run, an internal reference sample was analyzed, which was a subsample of a large 4 L sample that was collected at the beginning of the cruise. The average value of this sample was 0.33 ± 0.013 nM dFe ($n = 18$). Three different SAFe reference samples (S ($n = 4$), $D1$ ($n = 7$), and $D2$ ($n = 5$)) were regularly analyzed early in the cruise and about every third station for the remainder of the cruise to conserve these scarce reference samples. Results for these reference samples are in good agreement with the consensus values published in May 2013 (http://www.geotraces.org/science/intercalibration/322-standards-and-reference-materials). During each run, a drift standard was analyzed to account for any sensitivity changes during a run. This was usually less than 5% and was not corrected for, but occasionally larger drift of up to 12% was observed and the results were adjusted accordingly.

2.5. Phytoplankton

To collect phytoplankton samples, seawater was filtered under low vacuum pressure (<5 mm Hg) onto Whatman glass-fiber filters (GF/Fs) with a diameter of 25 mm and a nominal pore size of 0.7 μm and funnels were rinsed onto the filters with filtered seawater. After filtration for determination of fluorometric Chl a concentration, filters were stored in 90% acetone (5 mL) in the dark for 24 h at $+4°C$ for shipboard pigment extraction prior to shipboard analysis before and after acidification using a Turner Designs 10AU fluorometer. Samples for Chl a were taken at all depths in the upper 100 m.

Filtered samples for high-performance liquid chromatography (HPLC) analysis were collected from two depths at each full station (10 m and either the depth of the subsurface Chl *a* maximum [SCM] or 50 m if no SCM was present). Samples were flash frozen in liquid nitrogen and stored at −80°C until analysis. Pigments were separated by HPLC (Waters 2695) with a Zorbax Eclipse XDB-C8 column (3.5 μm particle size), using the method of Van Heukelem and Thomas (2001), modified after Perl (2009). After identification based on retention time and diode array spectroscopy (Waters 996), pigments were manually quantified using standards for all used pigments (DHI lab products). Phytoplankton community composition was estimated from HPLC pigments using the CHEMTAX analysis package (Alderkamp et al., 2015; Mackey et al., 1996) with a priori knowledge of the prior light environment and taxa present in the sample (FlowCam analysis). Based on FlowCam analysis, initial pigments included those for *Phaeocystis antarctica* (chlorophyll *c*3, chlorophyll *c*2, 19′-butanoyloxyfucoxanthin, fucoxanthin, and 19′-hexanoyloxyfucoxanthin), diatoms (chlorophyll *c*2 and fucoxanthin), dinoflagelates (peridinin), cryptophytes (alloxanthin), and chlorophytes (chlorophyll *b*, neoxanthin, and violaxanthin), with all pigments normalized by Chl *a* (Higgins et al., 2011; van Leeuwe et al., 2014).

We studied the photosynthetic response of natural phytoplankton assemblages to variations in light intensity by performing 221 photosynthesis versus irradiance (*P-E*) analyses, using methods described in Arrigo et al. (2010). From each *P-E* curve, we determined maximum biomass-specific photosynthetic rate (P^*_m), photosynthetic efficiency (α^*), photoinhibition (β^*), and the photoacclimation parameter ($E_k = P^*_m/\alpha^*$). *P-E* parameters were typically assessed at the same two depths at which HPLC samples were collected.

Phytoplankton variable fluorescence was measured in triplicate using a FIRe fluorometer (Fluorescence Induction and Relaxation System; Satlantic LP) at every station and a PAM fluorometer (Pulse Amplitude Modulated; Water-PAM, Heinz Walz) at every full station. Samples were dark acclimated on ice for 30 min (Alderkamp et al., 2012) prior to the determination of the maximum efficiency of photosystem II (Fv/Fm).

2.6. Satellite Remote Sensing
Daily sea ice cover from the period 1998 to 2016 was derived from the Special Sensor Microwave Imager available from the National Snow and Ice Data Center (NSIDC; https://nsidc.org).

Horizontal distributions of surface Chl *a* were determined from 8 day mean (9 km resolution) imagery from the Sea-viewing Wide Field-of-view Sensor (SeaWiFS) and MODerate Resolution Imaging Spectroradiometer (MODIS) for the period 1998–2016. For the years 1998–2002, surface Chl *a* concentrations were determined from Level 3 SeaWiFS ocean color data (Reprocessing R2014.0) using the OC4v6 algorithm (http://ocean-color.gsfc.nasa.gov/cms/reprocessing/OCReproc20100SW.html) a modified version of the OC4v4 algorithm (O'Reilly et al., 1998). For the years 2003–2016, surface Chl *a* concentrations were determined from Level 3 MODIS Aqua ocean color data (Reprocessing R2014.0) using the OC3Mv6 algorithm (O'Reilly et al., 2000). Although there is some debate about the accuracy of remotely sensed Chl *a* concentrations in the Southern Ocean (Haëntjens et al., 2017; Johnson et al., 2013), we are using them here only to characterize the annual cycle so determining absolute concentrations is not required.

2.7. Velocity Profiles
Velocity profiles were calculated using a combination of Acoustic Doppler Current Profiler (ADCP) data and CTD measurements. ADCP data were taken from two hull-mounted Ocean Surveyor instruments (Teledyne RD Instruments) measuring at 38 (OS38) and 150 (OS150) kHz (both narrowband configuration). ADCP measures the relative velocity of particles in the water. In general, higher frequencies give better resolution but do not penetrate as far into the water column. Data were processed using standard CODAS (Common Ocean Data Access System) techniques (http://currents.soest.hawaii.edu/docs/adcp_doc/index.html). Useable data from the OS38 and OS150 extended to approximately 1 km and 200 m depth, respectively, at 50 and 25 m vertical resolution. Between each pair of stations, an average velocity profile was calculated from each ADCP instrument. These were compared with a velocity profile between stations assumed from thermal wind balance using potential density measurements at each station. Thermal wind balance gives information on the vertical shear of the current assuming a small Rossby number, and therefore requires knowledge of a constant offset value. Here we used both ADCP measurements to give a best fit estimate of this constant offset for each station; if valid measurements from each instrument existed, the offset was calculated from both weighted by their respective residuals.

3. Results

3.1. Sea Ice Cover

The mean sea ice concentration (1998–2016) within our study region (an area within 100 km of the box bounded by Lines 200 and 700, denoted by the dashed lines in Figure 1) varied significantly throughout the year. Consequently, the mean open water area ranged from a minimum of ~170,000 km^2 in August/September to a maximum of ~332,000 km^2 in December/January (Figure 2a). The annual peak in open water area arrived approximately one month sooner in nonshelf (>500 m depth) waters (December, Figure 2b) than it did on the shelf (January, Figure 2c) due to earlier sea ice melt. On average, initiation of sea ice formation in the austral autumn began a few weeks earlier on the shelf (early May) than in nonshelf waters (late May). The annual cycle of open water area for 2014–2015, the year the Phantastic II cruise was conducted, was very similar to the 1998–2016 mean described above in both the nonshelf and shelf regions of our study area. The primary difference was that 2014–2015 exhibited a more rapid freeze-up in the austral autumn than the longer-term mean (Figures 2a–2c).

Sea ice concentrations during Phantastic II were generally highest in the southern portion of our study region at the time of sampling (Figure 3), with maximum concentrations approaching 100% along both Lines 200 and 300 but only 30% in the northernmost Line 700, which was mostly ice free. In addition, while the westernmost 100 km of each line was largely ice free, sea ice concentrations gradually increased shoreward, eventually peaking just inside the shelf break (<500 m).
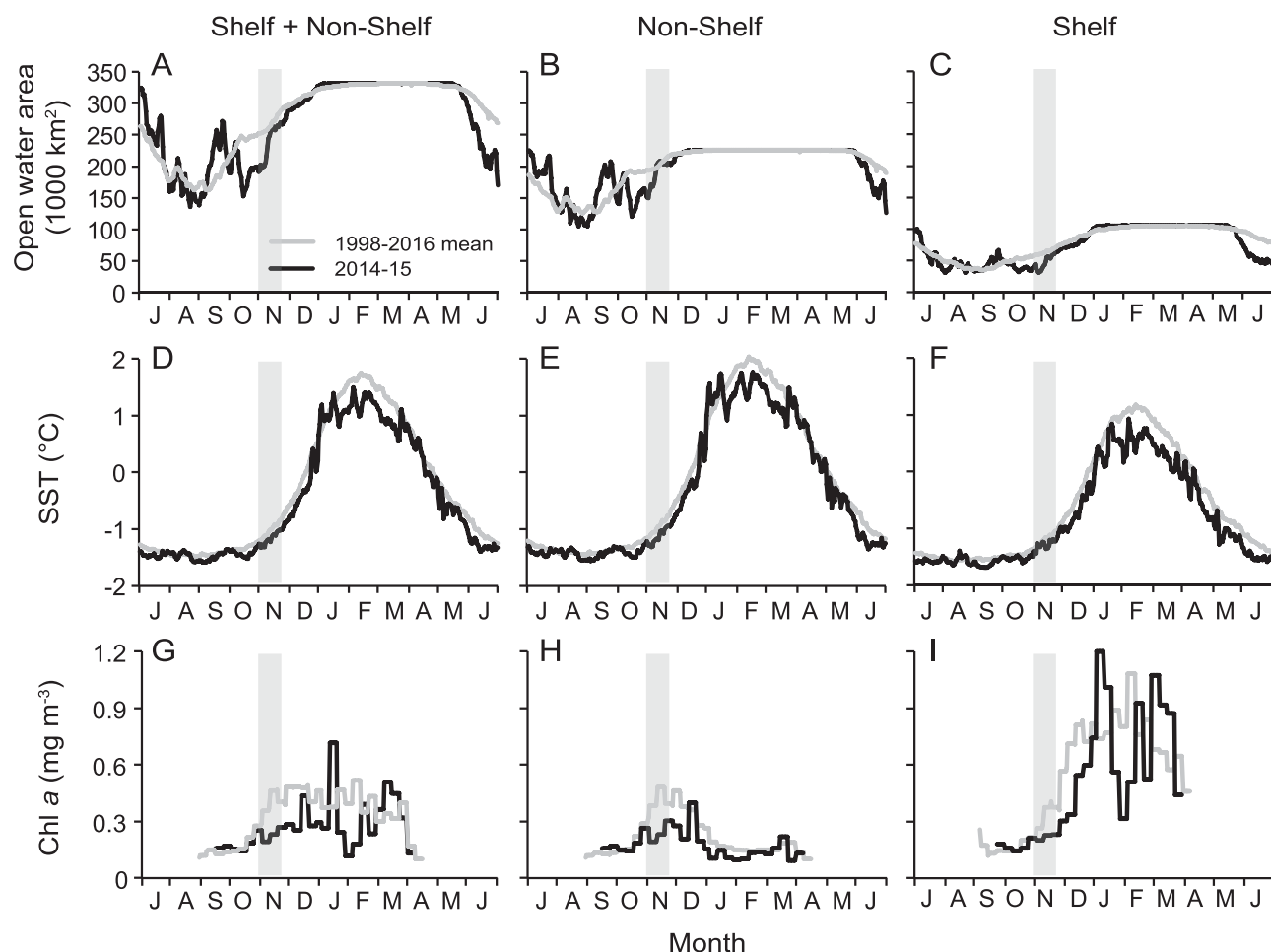

Figure 2. Annual cycle of open water area, sea surface temperature, and Chl *a* concentration for our study area in shelf + nonshelf waters, nonshelf waters only, and shelf waters only. The black lines represent values during the year of our cruise (2014–2015) and the gray lines are the means for 1998–2016. Vertical gray rectangles denote the timing of the Phantastic II cruise in 2014.
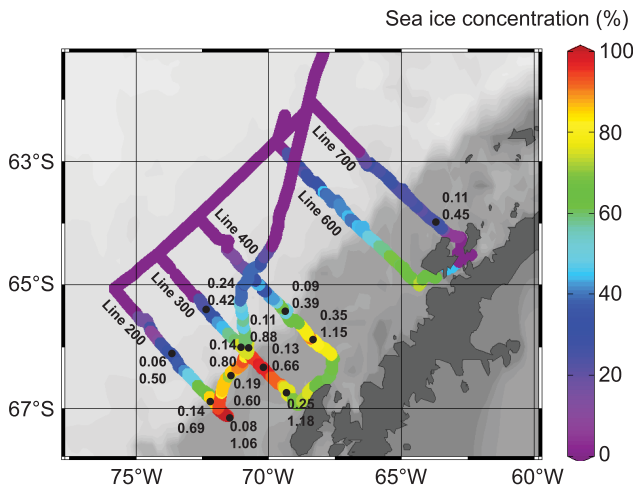
Figure 3. Satellite-derived sea ice concentrations along our cruise track. Also shown is the snow depth (m, top number) and ice thickness (m, bottom number) for 12 ice stations sampled during Phantastic II (black dots).

The mean sea ice thickness in our study region, based on the twelve ice stations sampled during Phantastic II, was 0.73 ± 0.28 m (Figure 3). There was a clear spatial pattern to sea ice thickness, which ranged from approximately 0.40 m at stations located near the ice edge to 1.15–1.20 m at stations sampled closer to shore. Snow cover exhibited no discernable spatial pattern, averaging 0.16 m and varying from 0.06 to 0.35 m across our sampling domain.

3.2. Hydrography

Sea surface temperature (SST). The satellite-based mean annual cycle of SST (1998–2016) in ice-free waters over our entire study region varied from a minimum of approximately $-1.49°C$ in August to $1.75°C$ in February (Figure 2d), with nonshelf waters tending to be warmer (Figure 2e) than those on the shelf (Figure 2f). This regional difference was relatively small in the austral winter when maximum SSTs in nonshelf and shelf waters were -1.46 and $-1.58°C$, respectively. However, by austral summer, the difference was much larger, with maximum SSTs in nonshelf waters being almost a degree warmer than waters on the shelf (2.03 and $1.18°C$, respectively). The relatively
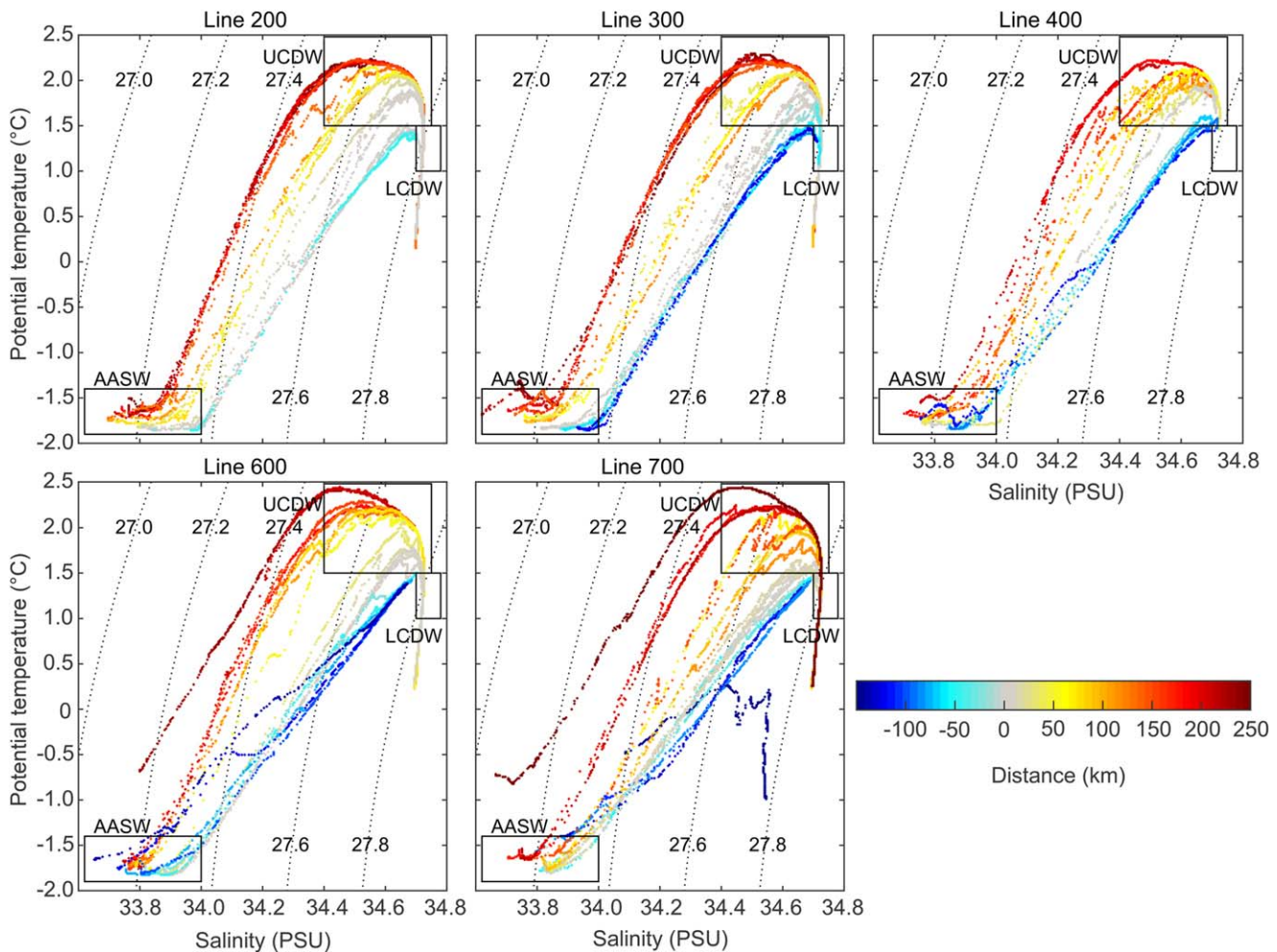

Figure 4. *T-S* diagrams for each line, with colors denoting distance from the shelf break (500 m isobath). Potential density contours are given in kg m^{-3}. Negative distances denote stations on the shelf.

high SSTs in nonshelf waters may help explain why sea ice there disappears about a month before the sea ice on the shelf.

Water masses. Temperature-salinity (*T-S*) plots for each transect (Figure 4) show that our study area was dominated by a mixture of Circumpolar Deep Water (CDW), a warm subsurface water mass characteristic of Antarctic Circumpolar Current (ACC) waters, and cold, fresh Antarctic Surface Water (AASW), defined here as waters with a potential temperature of $< -1.4°C$ and salinity <34. CDW is typically partitioned into upper (UCDW) and lower (LCDW) components, where UCDW encompasses a temperature maximum and oxygen minimum, and LCDW is characterized by a salinity maximum. In our study region, we defined UCDW as water with potential temperature $>1.5°C$ and salinity between 34.4 and 34.7 and LCDW as water with potential temperature between 1.0 and 1.5°C and salinity >34.7. Note that the absence of LCDW waters in Transect 400 is because all CTD casts on this transect were restricted to depths <750 m.

2-D sections of potential temperature, salinity, potential density, and oxygen concentration across Lines 200 and 600 (Figure 5) show the typical depth domains for both UCDW (200–800 m) and LCDW (800–2,000 m) in our study region. We also see the influence of UCDW and, in many cases, LCDW in waters over the continental shelf, although this influence does not extend far shoreward of the shelf break (25–50 km).

Fronts. Historically, our study region in the wAP is influenced by a number of different oceanographic fronts (Figure 1) as defined by Orsi et al. (1995). The southern boundary of the ACC (SBACC) is the southern terminus of water with CDW characteristics, which is approximately at the location of the continental shelf break in the wAP. In the wAP region, the SBACC and the southern ACC front (SACCF) are typically 50–200 km
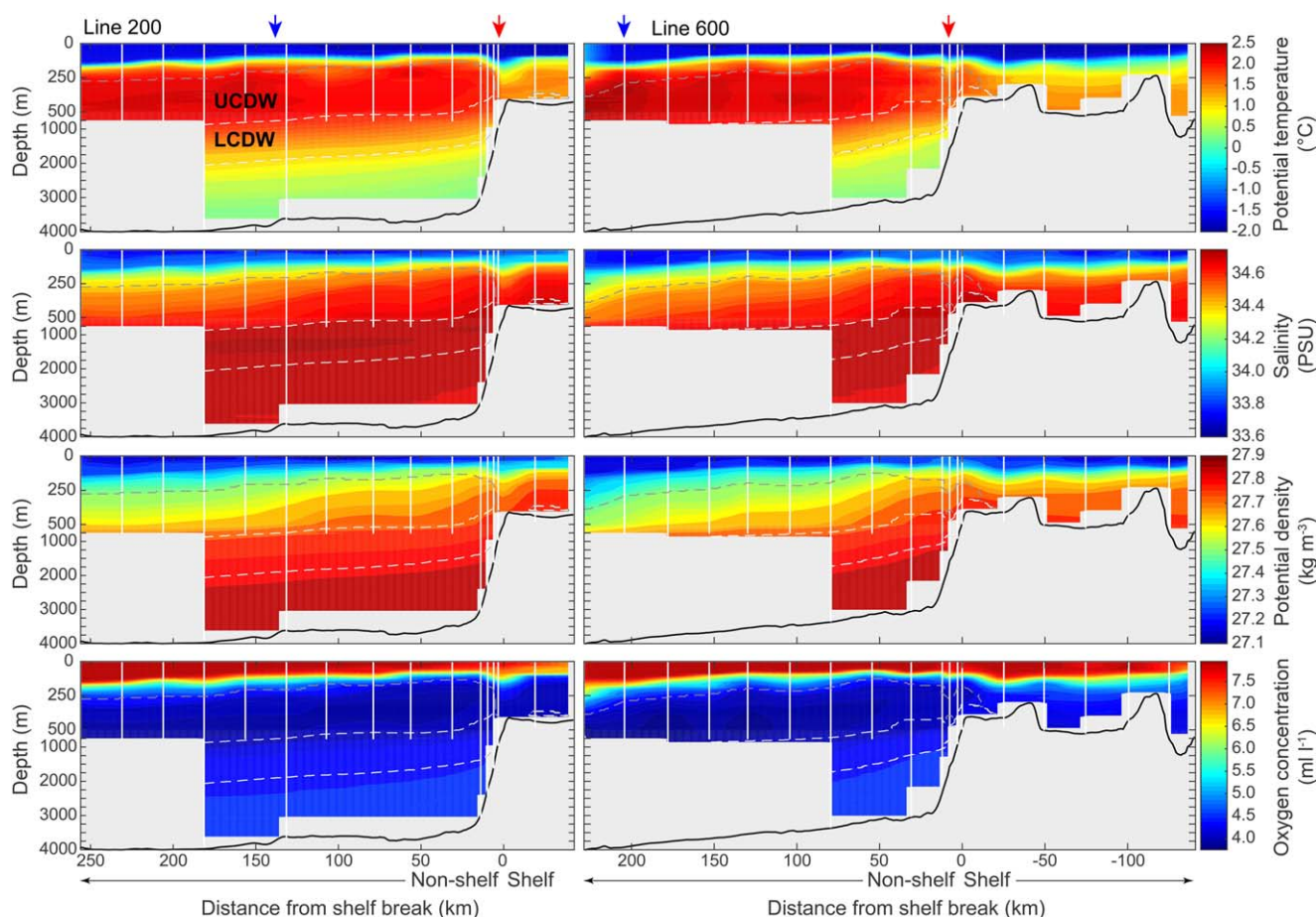
Figure 5. Potential temperature, salinity, potential density, and oxygen concentration for Lines 200 and 600. Values are interpolated between stations denoted by white lines. Black line gives bathymetry. Upper Circumpolar Deep Water (UCDW) lies between the gray and white dashed contours and Lower Circumpolar Deep Water (LCDW) lies between the two white dashed contours. Red arrows denote the central position of the SBACC. Blue arrows denote the central position of the SACCF. Negative distances denote stations on the shelf.
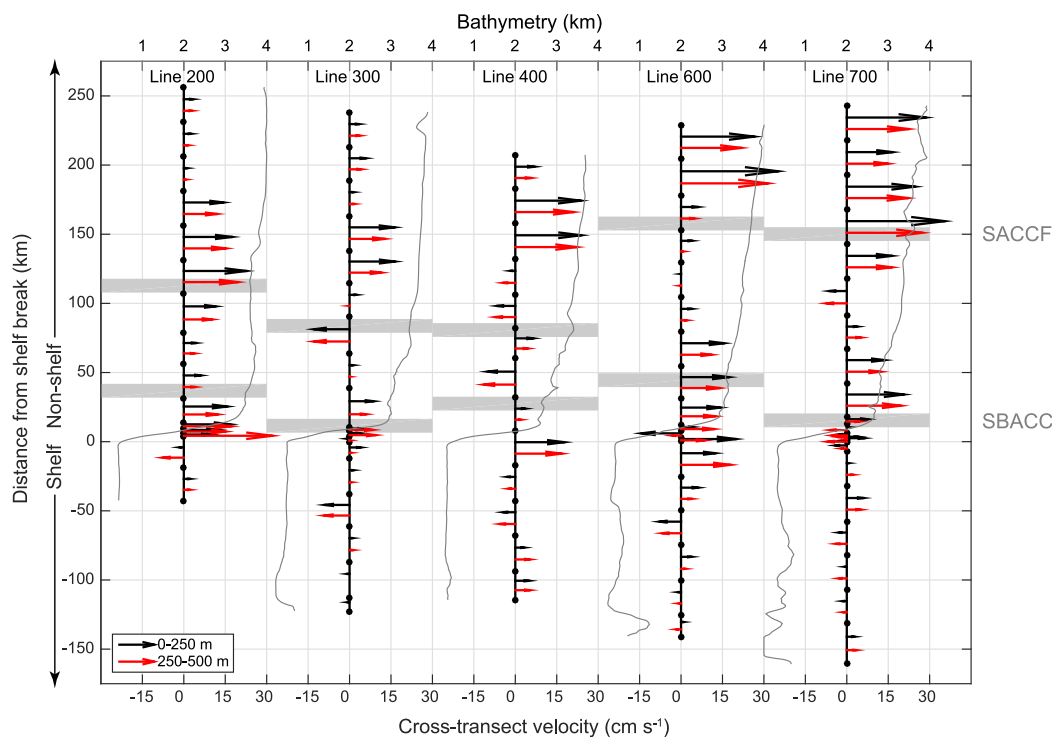
**Figure 6.** Geostrophic velocity between stations (black dots on each black line) from ADCP values at depths of 0–250 m (black arrows) and 250–500 m (red arrows) for each line. Thin gray lines give the bathymetry for each line. Gray rectangles on each line denote climatological locations of the SBACC (nearshore) and the SACCF (offshore) as given in Orsi et al. (1995); see also Figure 1.

apart, and were well-resolvable during our cruise (Figure 5). The Polar Front, associated with a sharp surface temperature gradient, is located further north and outside of our study area (Figure 1).

The frontal structure seaward of the shelf break is shown in the *T-S* diagrams (Figure 4). Stations between fronts have similar water mass characteristics and overlap each other in *T-S* space, whereas stations separated by a frontal jet show sharp differences in their *T-S* properties, becoming abruptly warmer, fresher, and less dense farther from the shelf. Stations overlapping a front typically show strong fine-scale interleaving in *T-S* (Joyce et al., 1978), indicated by a jagged structure largely along isopycnals (e.g., Line 400, 60 km; Line 700, 150 km). Locations of these frontal structures can also be seen as large horizontal gradients of potential density in our 2-D sections (Figure 5). The jet associated with the shelf break is particularly strong, as indicated by the classic chevron (v-shape) in potential density (Jacobs, 1991) seen at the shelf break in Lines 200 and 600 (Figure 5, near the red arrow).

The positions of the SACCF and SBACC during our study did not precisely align with the locations given by Orsi et al. (1995). We calculated the along-shelf mean geostrophic velocity between each pair of stations in the upper 500 m assuming thermal wind balance with an offset determined by average ADCP velocity measurements between each pair of stations. We found an "eastward" (in the direction of the ACC, which in this region is approximately northeast) current 100–250 km from the shelf break, and a separate "eastward" current associated with the shelf break (Figure 6). Compared with climatological locations for the SACCF and SBACC front (Figures 1 and 6), the SACCF location during our study was shifted equatorward in most transects, while a current associated with the SBACC was close to its climatological position (Figure 6).

3.3. Nutrient Concentrations

Over most of our study area, concentrations of NO_3^- and PO_4^{3-} were greatest within subsurface waters of the UCDW (Figure 7), with maximum concentrations of approximately 36 and 2.43 μM, respectively. The depth of the nutrient maximum in nonshelf waters varied with distance along each transect, decreasing from 300–400 m in the west to 150–200 m near the shelf break. This general spatial pattern contrasts with that of
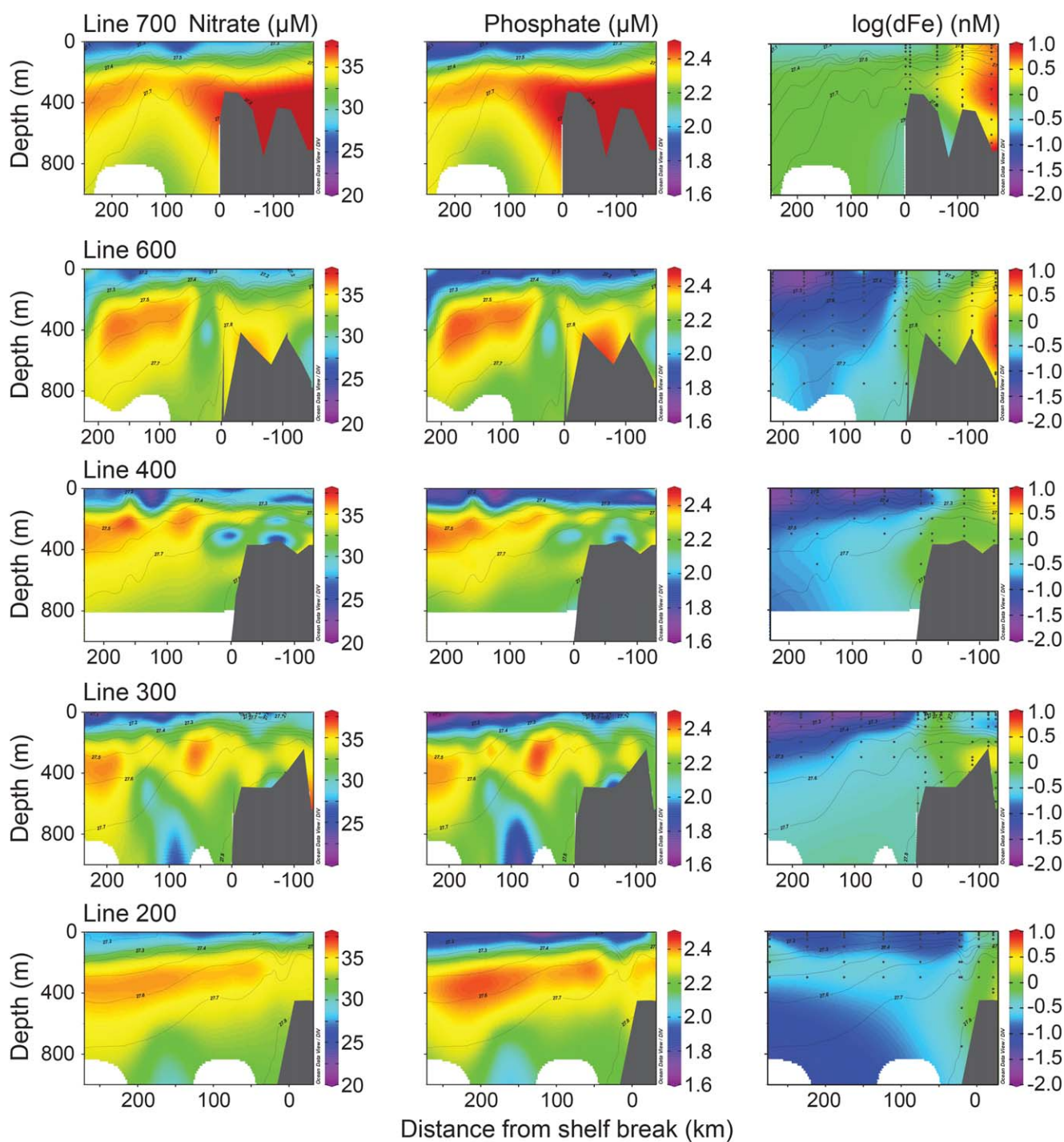
Figure 7. Vertical sections of NO_3^-, PO_4^{3-}, and dFe for the five lines sampled during Phantastic II. Black lines denote isopycnals every 0.1 kg m^{-3}. Negative distances denote stations on the shelf.

Si(OH)$_4$ (data not shown), which, while high in nonshelf waters within UCDW (40–80 μM), was generally much higher on the shelf (>100 μM). Macronutrient concentrations were high in near-surface waters at the time of our cruise, with minimum NO_3^- and PO_4^{3-} concentrations of 20 and 1.6 μM, respectively, well above levels that would be considered limiting for phytoplankton growth.

Unlike macronutrients, concentrations of dFe in nonshelf waters were extremely low, with concentrations often well below 0.1 nM (Figure 7). In general, dFe concentrations increased with depth to about 0.15 nM at

300 m and to 0.2–0.3 nM at 750 m. Over the continental shelf, dFe concentrations were much higher, exceeding 1 nM at all lines except 200 and reaching as high as 8.8 nM along Lines 600 and 700. Over the shelf, elevated dFe concentrations were observed near the surface as well as near the bottom, indicating the presence of both surface and sedimentary dFe sources, the latter of which is supported by observations of elevated Mn concentrations in deeper waters over the shelf (data not shown).
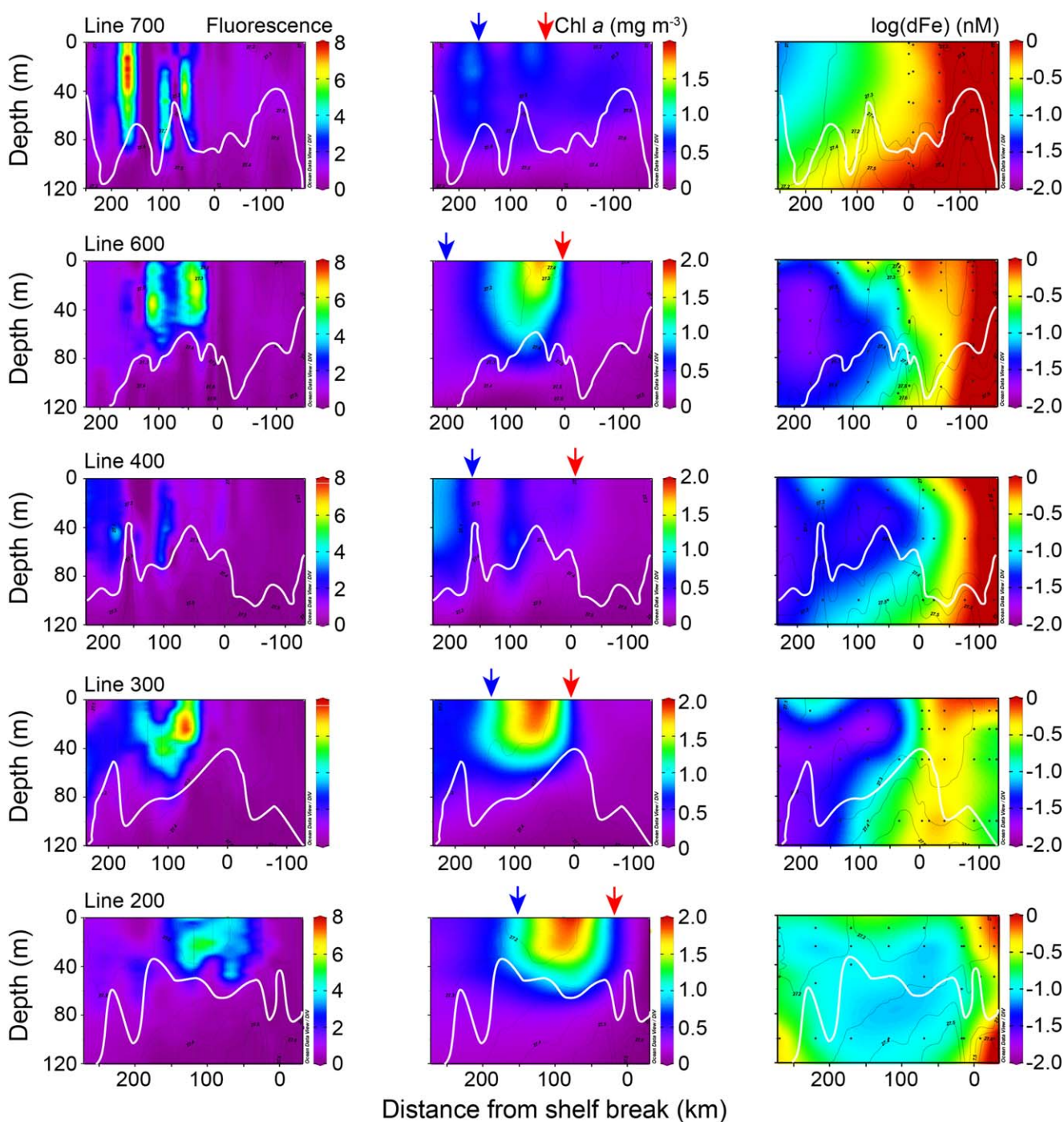
Figure 8. Vertical sections of CTD fluorescence, Chl a, and dFe in the upper water column for the five lines sampled during Phantastic II. White lines denote the depth of the mixed layer. Red arrows denote the central position of the SBACC. Blue arrows denote the central position of the SACCF. Black lines denote isopycnals every 0.1 kg m^{-3}. Vertical gray lines in fluorescence plots denote location of CTD profiles. Negative distances denote stations on the shelf.

3.4. Mixed Layer Depth

Springtime MLD varied from 40 to 120 m along each of the five lines sampled during Phantastic II (Figure 8). The relatively fast moving waters ($\sim$15 cm s^{-1}) associated with both the SBACC and SACCF generated a great deal of variability in MLD, which exhibited both local deepening to approximately 100–120 m and shoaling to 40–60 m, often over relatively short horizontal length scales (10s of km). The impact of these fronts on water column instability was also evidenced by the increased upward tilt of the isopycnals in the vicinity of the fronts (Figure 8). Within the relatively quiescent region between these two energetic fronts (150–200 km, Figure 6), MLD was generally much shallower (as shallow as 40 m) with slightly stronger stratification (Figure 8). However, stratification throughout our study area was still relatively weak this early in the melt season, so MLD is likely to be quite variable until the buoyancy of surface waters is increased by the addition of freshwater (primarily) or solar heating later (secondarily) in the spring and summer.

3.5. Phytoplankton

3.5.1. Biomass

The mean annual cycle of phytoplankton biomass between 1998 and 2016 in our study region, when expressed as the concentration of Chl a derived from satellite ocean color data, exhibits a typical spring bloom pattern, increasing rapidly from a minimum of 0.2 mg m^{-3} in mid-October to almost 0.6 mg m^{-3} in early November (Figure 2g). This mean value includes a substantial amount of spatial variability, with concentrations in excess of 10 mg m^{-3} observed in some locations. Averaged over the entire study region, Chl a persisted at this level for nearly five months, until the end of March, at which time concentrations rapidly dropped to 0.1 mg m^{-3}. The cause for this extended bloom period over the entire study region can be seen when nonshelf and shelf waters are considered separately. In nonshelf waters, the phytoplankton bloom begins in October, reaches a peak biomass of 0.5 mg m^{-3} by November, but is over by January (Figure 2h). In contrast, the phytoplankton bloom on the shelf does not begin until November and peaks in January or February, attaining Chl a concentrations (1.1 mg m^{-3}) that are twice as high as those in nonshelf waters, eventually declining in March (Figure 2i). Given the predominantly north-south direction of the prevailing currents in this region (Figure 6), there is not likely to be much exchange of material between the shelf and nonshelf blooms. It is the combination of an early bloom in nonshelf waters and a later bloom on the shelf that results in the persistently elevated values when phytoplankton biomass is averaged over our entire study region along the wAP.

During 2014–2015, the year of the Phantastic II cruise to the wAP, phytoplankton biomass exhibited spatial and temporal patterns that were similar to the 18 year mean, although satellite-based surface Chl a concentrations were generally lower and more variable than average throughout our study region (Figures 2g–2i). Given that we sampled the wAP early in the phytoplankton growth season during Phantastic II (Figure 2), surface concentrations of Chl a in situ were relatively low (0.1–0.3 mg m^{-3}, in good agreement with satellite data) over most of our study region at the time of sampling (Figure 8). However, there were regions of enhanced phytoplankton biomass throughout the wAP, especially along Lines 200, 300, and 600, in nonshelf waters just seaward of the shelf break. While Chl a concentrations were <0.3 mg m^{-3} at the surface and <40 mg m^{-2} within the upper 100 m over most of our study area, concentrations within the early blooms along these three lines were significantly higher ($p <$0.05) than those on the shelf, reaching values of up to 2.3 mg m^{-3} and 147 mg m^{-2}. The volume of the blooms varied somewhat between transects, but in general, they extended vertically from the surface to a depth of 40–60 m and horizontally for 100–150 km. Accumulation of particulate organic nitrogen was consistent with the depletion of nutrients in surface waters, suggesting that grazing losses were minimal this early in the phytoplankton bloom. Phaeopigment concentrations were also low, providing further evidence for low grazing pressure at this time.

The other two lines (400 and 700) also exhibited modest evidence of enhanced phytoplankton accumulation seaward of the shelf break in both the discrete pigments and the higher vertical resolution CTD fluorometer data, but to a lesser degree than the blooms observed along Lines 200, 300, and 600 (Figure 8). These enhanced Chl a features on Lines 400 and 700 were narrower (25–50 km) and extended deeper in the water column than the more intense blooms sampled along the other lines, with maximum Chl a concentrations of $\sim$1.3 mg m^{-3} extending to a depth of approximately 80 m (120 mg m^{-2}).

3.5.2. Phytoplankton Community Composition

Almost identical patterns of phytoplankton community composition were observed in both surface (2–10 m) and subsurface (25–50 m) waters throughout our study area, so only surface data are presented here.

Diatoms and haptophytes (microscopic analysis showed these haptophytes to be mostly a mix of single celled and colonial *P. antarctica*) were by far the two most abundant phytoplankton taxa observed in the wAP during Phantastic II (Figure 9). The percent contribution by these two taxa to total phytoplankton biomass was positively correlated with distance from shore ($R = 0.62$, $p < 0.05$) throughout the wAP. In nonshelf waters, the sum of these two taxa consistently exceeded 90% of total phytoplankton biomass. On the shelf, the dominance by these two taxa was reduced, although they still comprised 60–99% of the total phytoplankton biomass at all but one station (44%). Cryptophytes and chlorophytes were occasionally significant components of the phytoplankton community during our study. Their distributions were negatively correlated with distance from shore ($R = 0.60$, $p < 0.05$ and $R = 0.48$, $p < 0.05$, respectively), often exceeding 10% of total biomass in nearshore waters on the shelf, particularly along the two northernmost transects (Lines 600 and 700). Dinoflagellates never made up more than a few percent of the phytoplankton community in either shelf or nonshelf waters.

The pattern of dominance by diatoms and *P. antarctica* varied regionally during Phantastic II. Diatom relative abundance in nonshelf waters was greatest in the south and decreased with decreasing latitude ($R = 0.36$, $p < 0.05$), while that of *P. antarctica* exhibited the opposite pattern ($R = -0.36$, $p < 0.05$). On the
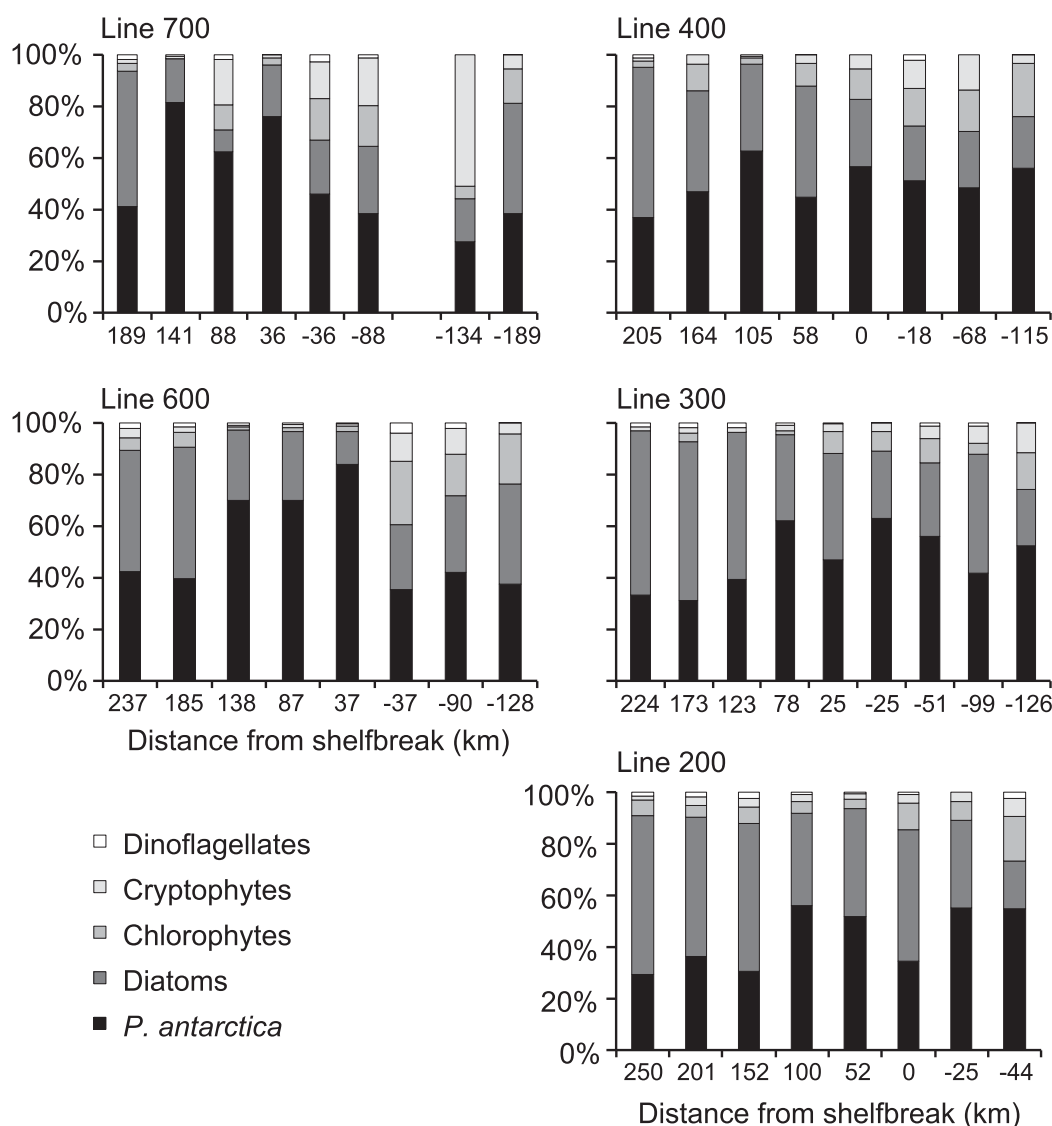

Figure 9. Phytoplankton community composition for the five lines sampled during Phantastic II as determined from HPLC pigment data using CHEMTAX. Negative distances denote stations on the shelf.

shelf, there was no significant latitudinal difference in diatom relative abundance, while *P. antarctica* abundance was greatest in the south and decreased toward the north ($R = 0.51$, $p < 0.05$). As a result, *P. antarctica* comprised an approximately equal proportion of the phytoplankton population in shelf and nonshelf waters in the southern portion of our study area (Lines 200, 300, and 400), but became more dominant in nonshelf waters further north (Lines 600 and 700). In addition, diatom abundance was negatively correlated with sea ice concentration ($R = -0.48$, $p < 0.05$), while *P. antarctica* exhibited a positive correlation ($R = 0.52$, $p < 0.05$). There was no statistically significant relationship between the abundance of *P. antarctica* or diatoms and either MLD or dFe concentration across our study region.

3.5.3. Phytoplankton Physiology

Fv/Fm. The maximum efficiency of photosystem II is a fairly good indicator of phytoplankton physiological state, with values below 0.4 generally indicating either nutrient or light stress and values over 0.4 generally suggesting a healthy population (Olson et al., 1999). During Phantastic II, mean values for Fv/Fm were surprisingly uniform and consistently above 0.5 in shelf and nonshelf waters and in ice-free and ice-covered regions (Table 1), indicating a healthy early bloom phytoplankton population over much of the wAP. There was no significant relationship between Fv/Fm and phytoplankton community composition.

Photosynthetic parameters. Like Fv/Fm, phytoplankton photosynthetic parameters in November were surprisingly uniform throughout the wAP and at the upper end of values reported previously for this and similar systems (Moline et al., 1998; Smith & Donaldson, 2015), indicative of a healthy phytoplankton community. The maximum biomass-specific photosynthetic rate ($P*_m$) averaged 3.30 ± 2.41 mg C mg^{-1} Chl *a* h^{-1} over our entire study region. Mean values on the shelf (3.97 ± 3.30 mg C mg^{-1} Chl *a* h^{-1}) were higher than those in nonshelf waters (2.93 ± 1.60 mg C mg^{-1} Chl *a* h^{-1}), although the difference was not statistically significant. The similarity in mean $P*_m$ was even more striking between ice-free and ice-covered waters, which exhibited values of 3.43 ± 1.88 and 3.19 ± 1.92 mg C mg^{-1} Chl *a* h^{-1}, respectively. There was no significant difference in $P*_m$ for any of the five lines sampled during Phantastic II, in either surface or subsurface waters (Table 1).

Photosynthetic efficiency ($\alpha*$) exhibited substantially more variability than $P*_m$, averaging 0.076 ± 0.146 mg C mg^{-1} Chl *a* h^{-1} (μmol photons m^{-2} s^{-1})$^{-1}$, but no distinct spatial pattern was observed. Values for $\alpha*$ in surface waters were similar to those in subsurface waters while values under the ice were higher than those in ice-free waters, although the difference was not significant (Table 1). Similarly, $\alpha*$ on the shelf was higher, but not significantly so, than $\alpha*$ in nonshelf waters.

Table 1
Mean (Standard Deviation) of Chl a Concentration, Photosynthetic Parameters ($P*_m$, $\alpha*$, and E_k) and Efficiency of Photosystem II (Fv/Fm) for Different Regions of the wAP

	Chl *a*	$P*_m$	$\alpha*$	E_k	Fv/Fm
All	0.55 (0.48)	3.30 (2.41)	0.076 (0.146)	75.7 (45.1)	0.53 (0.08)
Line 200, surface	0.81 (0.75)	1.92 (0.60)	0.028 (0.015)	88.4 (54.2)	0.51 (0.09)
Line 300, surface	0.72 (0.60)	3.33 (2.16)	0.045 (0.036)	86.4 (44.1)	0.49 (0.08)
Line 400, surface	0.37 (0.24)	3.57 (1.64)	0.042 (0.011)	89.5 (39.1)	0.55 (0.06)
Line 600, surface	0.52 (0.41)	2.28 (0.72)	0.025 (0.010)	91.7 (7.60)	0.52 (0.11)
Line 700, surface	0.55 (0.38)	3.49 (2.79)	0.045 (0.033)	97.6 (75.9)	0.52 (0.10)
All, surface	0.60 (0.50)	3.53 (1.96)	0.043 (0.026)	90.7 (49.7)	0.52 (0.09)
Line 200, subsurface	0.66 (0.76)	4.35 (5.26)	0.104 (0.166)	68.4 (33.8)	0.55 (0.05)
Line 300, subsurface	0.49 (0.36)	3.36 (1.78)	0.125 (0.210)	65.3 (49.1)	0.56 (0.07)
Line 400, subsurface	0.37 (0.32)	4.65 (2.64)	0.234 (0.379)	52.6 (45.3)	0.52 (0.02)
Line 600, subsurface	0.48 (0.42)	2.44 (0.48)	0.039 (0.012)	64.0 (10.5)	0.53 (0.08)
Line 700, subsurface	0.49 (0.34)	3.05 (1.30)	0.070 (0.048)	56.5 (30.7)	0.57 (0.09)
All, subsurface	0.50 (0.44)	4.37 (2.78)	0.119 (0.199)	61.2 (35.1)	0.55 (0.07)
Nonshelf	0.79 (0.53)	2.93 (1.60)	0.047 (0.034)	77.6 (37.9)	0.50 (0.07)
Shelf	0.28 (0.17)	3.97 (3.30)	0.127 (0.230)	72.6 (56.5)	0.60 (0.04)
Open water	0.51 (0.32)	3.43 (1.88)	0.055 (0.037)	86.5 (59.2)	0.50 (0.08)
Under ice	0.33 (0.41)	3.19 (1.92)	0.092 (0.192)	71.5 (37.6)	0.55 (0.08)

Note. Chl *a* (mg m^{-3}), $P*_m$ (mg C mg^{-1} Chl *a* h^{-1}), $\alpha*$ (mg C mg^{-1} Chl *a* h^{-1} (μmol photons m^{-2} s^{-1})$^{-1}$), E_k (μmol photons m^{-2} s^{-1}), and Fv/Fm (dimensionless).

As a consequence of the spatial consistency in both P^*_m and α^*, the photoacclimation parameter (E_k) exhibited very little variation across the wAP, averaging 75.7 ± 45.1 μmol photons m^{-2} s^{-1}. This value is remarkably similar to the mean light level we measured in the upper 40 m of the water column (the shallowest mixed layer we observed) over our entire study area (74.1 ± 84.2 μmol photons m^{-2} s^{-1}). Deeper mixed layers, which were common within our study region (Figure 8), had mean light levels well below E_k (mean light in the upper 80 m was only 39.3 ± 45.3 μmol photons m^{-2} s^{-1}), especially beneath sea ice (<10 μmol photons m^{-2} s^{-1}). As expected because of their lower light levels, mean E_k values in subsurface waters, on the shelf, and under the ice were lower than those in corresponding surface waters, nonshelf waters, and ice-free waters, respectively, although the differences were neither large nor statistically significant (Table 1).

4. Discussion

The wAP is a physically complex region of the Southern Ocean that is influenced by seasonal sea ice cover, energetic currents and fronts, dynamic MLDs, and highly variable bottom topography. These factors combine to modulate the light environment and nutrient concentrations of surface waters, producing the varied mosaic of pelagic environments that have been well described for the austral summer months (Ducklow et al., 2013; Garibotti et al., 2005; Marrari et al., 2008; Moreau et al., 2015; Trimborn et al., 2015). Our study shows that, despite this dynamic environment, phytoplankton physiological state in spring was surprisingly uniform throughout the wAP, likely due to the ample nutrient supplies that were available at that time and the early stage of the phytoplankton growth season when resource requirements are still relatively low. Furthermore, in contrast to the summer months when phytoplankton distributions are controlled primarily by nutrient availability, resulting in extremely high phytoplankton biomass near the coast on the shelf (Garibotti et al., 2005; Trimborn et al., 2015; Vernet et al., 2008), light appears to be the most important factor controlling phytoplankton growth in the wAP during spring. This is illustrated by our observations that light levels were low beneath the ice compared to measured values for E_k, suggesting that sea ice cover controlled bloom timing and location on the shelf while mixed layer dynamics played an important role in nonshelf waters.

4.1. Nutrient Distributions

Like observations made in summer, our study showed evidence of a strong SACCF and SBACC in the wAP, as evidenced by regions of energetic flow (Figure 6) and local deep mixing (Figure 8). The intrusion of the SBACC (the southern limit of CDW) onto the continental shelf can impact spring phytoplankton bloom development and also lead to glacial melting (Martinson et al., 2008; Martinson & McKee, 2012; Moffat et al., 2009). We found small amounts of warm water with UCDW characteristics on the shelf in all of the transects (Figure 4), likely resulting from eddies mixing water masses across the shelf break (Moffat et al., 2009), suggesting that the SBACC intrusion was ubiquitous across the shelf in our study.

However, in addition to bringing warm waters onto the shelf, UCDW also contains high micronutrient and macronutrient concentrations that fuel the growth of phytoplankton in both shelf and nonshelf waters (Alderkamp et al., 2012; Arrigo et al., 2015; Gerringa et al., 2012). During our study, high concentrations of NO_3^- and PO_4^{3-} had been brought closest to the ocean surface in the nonshelf region between the SACCF and the SBACC (Figures 6 and 7). Winter mixing entrained these high subsurface nutrient inventories into surface waters, resulting in our observations of prebloom macronutrient concentrations in excess of 1.6 μM PO_4^{3-} and 20 μM NO_3^-. Some $Si(OH)_4$ was probably also entrained into surface waters in this manner, but during our study, concentrations of $Si(OH)_4$ (and Mn, a tracer of lithogenic resuspension) were always highest on the shelf, suggesting that resuspension of sediment inventories was a more important process in shallower waters (Arrigo et al., 2015; Gerringa et al., 2012). Consistent with numerous other observations from the Antarctic (Arrigo et al., 2000; Gordon et al., 2000; Hoppema et al., 2015), the prebloom macronutrient levels in surface waters we observed during Phantastic II were well above concentrations required to sustain maximum phytoplankton growth rates, once limitation by other scarce resources was alleviated (e.g., light and micronutrients).

Like the more abundant macronutrients, it is generally assumed that deep winter mixing also replenishes the surface layer with dFe (Tagliabue et al., 2014). However, we found that during our occupation of the wAP early in the austral summer, the dFe concentrations in nonshelf waters were quite low, showing little

sign of having been replenished by vertical mixing during the past winter (Figure 7), except perhaps along Line 200 where a dFe concentration of 0.8 nM was observed at 120 m (Figure 8). A closer look at the upper water column of nonshelf waters along Lines 200, 300, and 600 (Figure 8) shows enhanced dFe concentrations in the upper 20 m (0.2–0.3 nM), coincident with the region of reduced sea ice cover (Figure 3). This suggests that melting sea ice, which can contain high concentrations of dFe (Lannuzel et al., 2016; Sedwick & DiTullio, 1997) and dFe-stabilizing organic ligands (Lannuzel et al., 2015), was the source of surface dFe in nonshelf waters, although there was no obvious freshwater lens associated with the layer of enhanced dFe, as evidenced in the relatively widely spaced density contours (Figure 8).

Prebloom concentrations of dFe were higher on the shelf, particularly in nearshore regions, suggesting that dFe was being supplied either from the sediments, from melting ice, or both (Arrigo et al., 2015; Gerringa et al., 2012; Planquette et al., 2011, 2013). Line 700 had very little sea ice over the shelf, so water column dFe was most likely derived from either the sediments or glacial melt (Raiswell, 2011; Raiswell et al., 2008). Steeply vertical isopycnals on the shelf in most of our transects (Figure 8) indicate a high degree of mixing, consistent with a UCDW or local sedimentary source of dFe that had been mixed into surface waters (Gerringa et al., 2012). In addition, the elevated surface dFe along Lines 200 and 300 in an area of the shelf with 100% sea ice cover suggests that glacial ice, rather than sea ice, may have been an important dFe source.

4.2. Phytoplankton Distributions

Phytoplankton blooms in the wAP have been studied extensively in recent decades (Ducklow et al., 2013), although most of the effort has been concentrated during the summer, with only a small amount of information about the development of phytoplankton blooms available in the austral spring (Moreau et al., 2010). Based on the results from Phantastic II, phytoplankton in both the surface and subsurface of shelf and nonshelf waters were physiologically competent and capable of rapid growth in the austral spring. In fact, we were somewhat surprised to find that, despite very low nonshelf dFe concentrations, phytoplankton in nonshelf waters showed no sign of dFe stress, which is usually manifested as a reduction in Fv/Fm (Behrenfeld & Milligan, 2012; Boyd & Abraham, 2001; Hopkinson et al., 2007) or an inverse relationship between Fv/Fm and absorption cross section of PSII (σ_{PSII}; Behrenfeld & Kolber, 1999, Hopkinson et al., 2007). Throughout the wAP, we observed uniformly high Fv/Fm and no relationship between Fv/Fm and σ_{PSII} (data not shown). These results contrast with other studies in the wAP that were conducted later in the summer and showed markedly reduced values for Fv/Fm in nonshelf waters (Trimborn et al., 2015) but higher values on the shelf (García-Muñoz et al., 2014; Hopkinson et al., 2007; Trimborn et al., 2015), and an inverse relationship between Fv/Fm and σ_{PSII} (Trimborn et al., 2015). Our results suggest that despite low initial dFe concentrations in nonshelf surface waters, there was still sufficient dFe being supplied to the early phytoplankton bloom during spring to maintain a healthy population, possibly from melting sea ice, similar to observations made previously in the Ross Sea (Sedwick et al., 2011).

Phytoplankton abundance in our study area during austral spring appeared to be related to a combination of physical factors, including the amount of sea ice cover, the positions of major oceanographic fronts, and MLD. Unlike Chl a concentrations often measured during the summer when phytoplankton are much more abundant on the continental shelf than in nonshelf waters (>10 mg m^{-3} and <1 mg m^{-3}, respectively; Trimborn et al., 2015; Varela et al., 2002; Vernet et al., 2008), Chl a concentrations during Phantastic II were generally low on the shelf, rarely exceeding 0.2 mg m^{-3}, despite high concentrations of macronutrients (Figure 7) and dFe (Figure 8). The low phytoplankton biomass we observed on the shelf is most likely a consequence of the high concentrations of sea ice at this time of year, which greatly reduced light transmission to surface waters (Selz et al., 2016) and decreased light levels to well below measured values for E_k. This conclusion is further supported by our observation that Chl a concentrations on the shelf only exceeded 0.5 mg m^{-3} along Line 700 where sea ice concentrations were consistently below 35% (Line 700, Figure 3).

In contrast to shelf waters of the wAP where Chl a concentrations were greatest in areas of reduced ice cover, Chl a concentrations seaward of the shelf break were highest in regions with a variable amount of sea ice cover (10–50%), rather than in nonshelf waters farther offshore that were relatively ice free (Figure 3). Unfortunately, even the reduced ice concentrations present during our study are too high to allow satellite detection of the phytoplankton bloom developing in waters below, which may partially explain why the satellite-based Chl a concentrations presented in Figure 2 and in Marrari et al. (2008) are lower than those presented here from in situ measurements. The coincidence between reduced sea ice concentrations and

increased Chl *a* suggests that we had observed a MIZ phytoplankton bloom that developed as a result of meltwater stratification induced by the retreat of melting sea ice (Smith & Nelson, 1986), perhaps associated with addition of dFe to surface water from melting sea ice (Lannuzel et al., 2015, 2016). However, closer inspection of our hydrographic data suggests that physical processes associated with the two major fronts in the region also played a large role in the spatial pattern of phytoplankton bloom development. This is consistent with observations made over a much smaller area during the austral spring and summer as part of the STERNA program in 1992, which also observed high phytoplankton biomass associated with frontal regions along the wAP, rather than associated with the sea ice edge (Turner & Owens, 1995).

Within the area of reduced sea ice cover, phytoplankton abundance was greatest in the area between the northward flowing SBACC and SACCF (Figure 8). This is best seen along Lines 200, 300, and 600 where the highest Chl *a* concentrations were clearly bounded by these two fronts. The intensified currents associated with the SBACC and SACCF generated a local deepening of the mixed layer to approximately 100–120 m, thereby reducing mixed layer light levels and presumably slowing phytoplankton growth rates. However, within the area between these two fronts, MLD was generally much shallower and slightly more stratified (Figure 8). As a result, mixed layer light levels were higher between the fronts (data not shown) and phytoplankton biomass accumulated at a faster rate than in waters either further inshore or offshore.

This pattern is not as clear in Lines 400 and 700 where phytoplankton abundance was much lower. There, a number of deep, narrow Chl *a* features correspond with greater MLDs, suggesting that these waters had recently mixed, carrying surface phytoplankton to depth and diluting their concentrations. Some of this deep mixing may have been generated by local winds, especially along Line 700 where ice cover was relatively low and Chl *a* concentrations on the shelf were higher than elsewhere. Thus, on the shelf, the development of the spring phytoplankton bloom in the wAP is inhibited by the presence of heavy sea ice on the shelf, while in nonshelf waters, the spring bloom is controlled by interactions between melting sea ice, which both enhances upper ocean stratification and possibly adds dFe to surface waters, and vertical mixing associated the SBACC and SACCF, which breaks down stratification but also brings nutrients up into surface waters.

4.3. Phytoplankton Community Composition

The spatial pattern of phytoplankton community composition observed in the wAP in austral spring during Phantastic II (Figure 9) agrees broadly with patterns observed previously in this region, but later in the summer. In both seasons, diatoms were abundant in shelf and nonshelf waters, although generally more so both off the shelf (Huang et al., 2012; Kavanaugh et al., 2015; Trimborn et al., 2015; Varela et al., 2002, but see Garibotti et al., 2005) and further south in the wAP region (Huang et al., 2012). *P. antarctica* abundance was greatest in nonshelf waters, especially further north (Trimborn et al., 2015). In addition, while cryptophytes were consistently a minor component of the phytoplankton community everywhere (Rodriguez et al., 2002; Trimborn et al., 2015; Varela et al., 2002), their abundance was greatest in more northern and inshore waters of the wAP where glacial melt is greatest, as reported previously by Huang et al. (2012).

The biggest difference in community composition between austral spring and summer appears to be in the degree of relative dominance by diatoms and *P. antarctica*. In spring, data from Phantastic II show that both diatoms and *P. antarctica* are relatively abundant in both shelf and nonshelf waters, with *P. antarctica* being most abundant in offshore waters further north and diatoms most abundant in offshore waters further south (Figure 9). On the shelf, chlorophytes and cryptophytes often accounted for 20% of total phytoplankton biomass, and reached as high as 40% in spring. In contrast, during summer, diatoms overwhelmingly dominate on the shelf, accounting for as much as 100% of the phytoplankton community (Trimborn et al., 2015). Few other taxa are found anywhere along the wAP, although blooms of *P. antarctica* have been observed (Rodriguez et al., 2002; Trimborn et al., 2015; Varela et al., 2002), but not consistently (Garibotti et al., 2003). Despite its presence throughout the wAP, particularly in offshore waters, *P. antarctica* relative abundance in summer (Trimborn et al., 2015) is far below levels we observed in the spring. Thus, diatoms appear to make up an increasingly dominant fraction of the phytoplankton community between spring and summer, as also observed at Rothera (Rozema et al., 2017).

Trimborn et al. (2015) attributed the enhanced abundance of *P. antarctica* in nonshelf waters to their higher Fe uptake rates, presumably stemming from a higher affinity for Fe, especially for single celled forms (Hassler & Schoemann, 2009). This allowed them to better compete with diatoms in this relatively low-dFe

environment during summer. At this same time, Trimborn et al. (2015) proposed that diatoms dominated the phytoplankton community on the shelf because of their higher intrinsic growth rates under conditions of high dFe concentration. This hypothesis is broadly consistent with distributions of dFe and phytoplankton community composition we measured during Phantastic II (more *P. antarctica* in nonshelf waters where dFe is low, significant abundance of diatoms everywhere). However, it does not explain why diatoms comprised a relatively larger fraction of the phytoplankton community in offshore waters in summer (Trimborn et al., 2015), when dFe levels would be expected to be even more limiting to phytoplankton growth and would be expected to favor *P. antarctica* to an even greater extent than in spring.

Perhaps the relative distributions of *P. antarctica* and diatoms in the wAP during spring have more to do with the distributions of sea ice than differences in dFe availability between shelf and nonshelf waters. Phytoplankton exhibited no evidence of Fe stress anywhere in our study region, and there was no relationship between phytoplankton community composition and dFe. Furthermore, diatom relative abundance was negatively correlated with sea ice concentration (–0.48, $p < 0.05$) while distributions of the low light form of *P. antarctica* were positively correlated with sea ice cover (0.52, $p < 0.05$), consistent with their ability to grow faster at lower light levels (Kropuenske et al., 2010). This suggests that the high relative abundance of *P. antarctica* on the shelf may be attributable to the more widespread sea ice observed there in the spring (Figure 3). This conclusion is supported by high concentrations of *P. antarctica* observed within sea ice during Phantastic II (Selz et al., 2016). Concentrated within a 0.1–0.2 m slush layer located between the top of the ice and the overlying snow cover, communities dominated by *P. antarctica* were more physiologically active than communities living elsewhere in the sea ice. Furthermore, the similarity in community composition between the sea ice and the water column suggests that *P. antarctica* from the ice may be released into the water column where they subsequently grow as phytoplankton. Selz et al. (2016) also showed that colonial *P. antarctica* sinks through the water column much faster than diatoms, perhaps explaining their relative scarcity in the wAP in summer (Trimborn et al., 2015). Thus, widespread sea ice appears to favor the growth of *P. antarctica* during spring while the loss of ice in summer favors the proliferation of the faster-growing diatoms.

5. Conclusions

Results from Phantastic II show that at the start of the spring bloom, the phytoplankton community is physiologically active and healthy throughout the wAP. Diatoms and *P. antarctica* are both widespread at this time, but other phytoplankton taxa are present in modest numbers on the shelf. As solar insolation increases during spring, heavy ice cover on much of the shelf prevents net phytoplankton growth in these nutrient-rich waters, except in the far north (Line 700) where sea ice concentrations are lower. In waters seaward of the shelf break with reduced ice cover, it is only in the area of reduced vertical mixing between the SBACC and SACCF where mixed layer light levels are sufficient in spring for net growth of physiologically competent phytoplankton (Figure 8). As phytoplankton biomass, consisting mostly of diatoms in the south and *P. antarctica* in the north, starts to accumulate within the bloom, any dFe in surface water that was available in early spring is rapidly consumed (Figure 7) and is likely replenished by dFe released from melting ice, allowing the bloom to progress.

In late austral spring, satellite data show that the phytoplankton bloom in nonshelf waters expands beyond the boundaries of the SBACC and SACCF (Marrari et al., 2008), presumably as a result of increasing surface ocean stratification. The most likely source of dFe fueling this additional phytoplankton growth seems to be melting sea ice or upwelling at the fronts, although this needs to be confirmed in situ. As austral spring moves into summer, the remaining sea ice disappears, first in nonshelf waters and then on the shelf (Figures 2a and 2b). At this time, the nonshelf bloom begins to decline and increased light availability, coupled with increased stratification (Garibotti et al., 2005) and reservoirs of dFe resulting from local mixing and movement of UCDW, facilitate the accumulation of high concentrations of phytoplankton biomass on the continental shelf (Figure 2i), consisting mostly of diatoms (Trimborn et al., 2015; Varela et al., 2002; Vernet et al., 2008).

These results shed important light on the possible controls of phytoplankton dynamics in the wAP during the critical spring-to-summer transition. Interactions between changing sea ice cover, nutrient delivery and vertical mixing appear to be the dominant controls on the growth of phytoplankton in the wAP during this

time. Interestingly, these components of the system are either undergoing or have the potential to undergo significant changes in the decades to come as temperatures in this region continue to rise and wind patterns due to changes in atmospheric pressure are altered (Cerrone et al., 2017; Stammerjohn et al., 2012; Thompson & Youngs, 2013). These changes could eventually impact the community structure and productivity of the phytoplankton on which the entire wAP ecosystem depends (Saba et al., 2014).

References

Alderkamp, A.-C., Mills, M. M., van Dijken, G. L., Laan, P., Thuroczy, C.-E., Gerringa, L., . . . Arrigo, K. R. (2012). Iron from melting glaciers fuels phytoplankton blooms in Amundsen Sea (Southern Ocean), Phytoplankton characteristics and productivity. *Deep Sea Research Part II: Topical Studies in Oceanography*, *71–76*, 32–48. https://doi.org/10.1016/j.dsr2.2012.03.005

Alderkamp, A.-C., van Dijken, G. L., Lowry, K. E., Connelly, T. L., Lagerström, M., Sherrell, R. M., . . . Arrigo, K. R. (2015). Fe availability drives phytoplankton photosynthesis rates during spring bloom in the Amundsen Sea Polynya, Antarctica. *Elementa: Science of the Anthropocene*, *3*, 43. https://doi.org/10.12952/journal.elementa.000043

Arrigo, K. R., DiTullio, G. R., Dunbar, R. B., Robinson, D. H., Van Woert, M., Worthen, D. L., & Lizotte, M. P. (2000). Phytoplankton taxonomic variability and nutrient utilization and primary production in the Ross Sea. *Journal of Geophysical Research*, *105*, 8827–8846.

Arrigo, K. R., Mills, M. M., Kropuenske, L. R., van Dijken, G. L., Alderkamp, A. C., & Robinson, D. H. (2010). Photophysiology in two major Southern Ocean phytoplankton taxa: Photosynthesis and growth of *Phaeocystis antarctica* and *Fragilariopsis cylindrus* under different irradiance levels. *Integrative and Comparative Biology*, *50*(6), 950–966. https://doi.org/10.1093/icb/icq021

Arrigo, K. R., van Dijken, G. L., & Strong, A. L. (2015). Environmental controls of marine productivity hot spots around Antarctica. *Journal of Geophysical Research: Oceans*, *120*, 5545–5565. https://doi.org/10.1002/2015JC010888

Behrenfeld, M. J., & Kolber, Z. S. (1999). Widespread iron limitation of phytoplankton in the South Pacific Ocean. *Science*, *283*, 840–843.

Behrenfeld, M. J., & Milligan, A. J. (2012). Photophysiological expressions of iron stress in phytoplankton. *Annual Review of Marine Science*, *5*, 4.1–4.30.

Boyd, P. W., & Abraham, E. R. (2001). Iron-mediated changes in phytoplankton photosynthetic competence during SOIREE. *Deep Sea Research Part I: Oceanographic Research Papers*, *48*, 2529–2550.

Cerrone, D., Fusco, G., Simmonds, I., Aulicino, G., & Budillon, G. (2017). Dominant covarying climate signals in the Southern Ocean and Antarctic sea ice Influence during the last three decades. *Journal of Climate*, *30*(8), 3055–3072.

Clarke, A., Meredith, M. P., Wallace, M. I., Brandon, M. A., & Thomas, D. N. (2008). Seasonal and interannual variability in temperature, chlorophyll and macronutrients in northern Marguerite Bay, Antarctica. *Deep Sea Research Part II: Topical Studies in Oceanography*, *55*, 1988–2006. https://doi.org/10.1016/j.dsr2.2008.04.035

Dong, S., Sprintall, J., Gille, S. T., & Talley, L. (2008). Southern Ocean mixed-layer depth from Argo float profiles. *Journal of Geophysical Research*, *113*, C06013. https://doi.org/10.1029/2006JC004051

Ducklow, H. W., Baker, K., Martinson, D. G., Quetin, L. B., Ross, R. M., Smith, R. C., . . . Fraser, W. R. (2007). Marine pelagic ecosystems: The West Antarctic Peninsula. *Philosophical Transactions of the Royal Society of London B*, *362*, 67–94. https://doi.org/10.1098/rstb.2006.1955

Ducklow, H. W., Fraser, W. R., Meredith, M. P., Stammerjohn, S. E., Doney, S. C., Martinson, D. G., . . . Amsler, C. D. (2013). West Antarctic Peninsula: An ice-dependent coastal marine ecosystem in transition. *Oceanography*, *26*(3), 190–203. https://doi.org/10.5670/oceanog.2013.62

García-Muñoz, C., Sobrino, L. M., Lubián, C. M., García, S., Martínez-García, P. & Sangrà, (2014). Factors controlling phytoplankton physiological state around the South Shetland Islands (Antarctica). *Marine Ecology Progress Series*, *498*, 55–71.

Garibotti, I. A., Vernet, M., & Ferrario, M. E. (2005). Interannual variability in the distribution of the phytoplankton standing stock across the seasonal sea-ice zone west of the Antarctic Peninsula. *Journal of Plankton Research*, *27*, 825–843.

Garibotti, I. A., Vernet, M., Ferrario, M. E., Smith, R. C., Ross, R. M., & Quetin, L. B. (2003). Phytoplankton spatial distribution patterns in the western Antarctic Peninsula (Southern Ocean). *Marine Ecology Progress Series*, *261*, 21–39.

Gerringa, L. J. A., Alderkamp, A.-C., Laan, P., Thuróczy, C.-E., de Baar, H. J. W., Mills, M. M., . . . Arrigo, K. R. (2012). Iron from melting glaciers fuels the phytoplankton blooms in Amundsen Sea (Southern Ocean): Iron biogeochemistry. *Deep Sea Research Part II: Topical Studies in Oceanography*, *71–76*, 16–31. https://doi.org/10.1016/j.dsr2.2012.03.007

Gordon, L. I., Codispoti, L. A., Jennings, J. C., Millero, F. J., Morrison, J. M., & Sweeney, C. (2000). Seasonal evolution of hydrographic properties in the Ross Sea, Antarctica, 1996–1997. *Deep Sea Research Part II: Topical Studies in Oceanography*, *47*(15–16), 3095–3117. https://doi.org/10.1016/S0967-0645(00)00060-6

Haëntjens, N., Boss, E., & Talley, L. D. (2017). Revisiting Ocean Color algorithms for chlorophyll *a* and particulate organic carbon in the Southern Ocean using biogeochemical floats. *Journal of Geophysical Research: Oceans*, *122*, 6583–6593. https://doi.org/10.1002/2017JC012844

Hassler, C. S., & Schoemann, V. (2009). Bioavailability of organically bound Fe to model phytoplankton of the Southern Ocean. *Biogeosciences*, *6*, 2281–2296.

Higgins, H. W., Wright, S. W., & Schluter, L. (2011). Quantitative interpretation of chemotaxonomic pigment data. In S. Roy, C. A. Llewellyn, E. S. Egeland, & G. Johnsen (Eds.), *Phytoplankton pigments: Characterization, chemotaxonomy and applications in oceanography*. Cambridge, UK: Cambridge University Press.

Hopkinson, B. M., Mitchell, B. G., Reynolds, R. A., Wang, H., Selph, K. E., Measures, C. I., . . . Barbeau, K. A. (2007). Iron limitation across chlorophyll gradients in the southern Drake Passage: Phytoplankton responses to iron addition and photosynthetic indicators of iron stress. *Limnology and Oceanography*, *52*, 2540–2554.

Hoppema, M., Bakker, K., van Heuven, S. M. A. C., van Ooijen, J. C., & de Baar, H. J. W. (2015). Distributions, trends and inter-annual variability of nutrients along a repeat section through the Weddell Sea (1996–2011). *Marine Chemistry*, *177*, 545–553.

Huang, K., Ducklow, H., Vernet, M., Cassar, N., & Bender, M. L. (2012). Export production and its regulating factors in the West Antarctica Peninsula region of the Southern Ocean. *Global Biogeochemical Cycles*, *26*, GB2005. https://doi.org/10.1029/2010GB004028

Jacobs, S. S. (1991). On the nature and significance of the Antarctic Slope Front. *Marine Chemistry*, *35*, 9–24.

Johnson, R., Strutton, P. G., Wright, S. W., McMinn, A., & Meiners, K. M. (2013). Three improved Satellite Chlorophyll algorithms for the Southern Ocean. *Journal of Geophysical Research: Oceans*, *118*, 3694–3703. https://doi.org/10.1002/jgrc.20270

Joyce, T. M., Zenk, W., & Toole, J. M. (1978). The anatomy of the Antarctic Polar Front in the Drake Passage. *Journal of Geophysical Research*, *83*, 6093. https://doi.org/10.1029/JC083iC12p06093

Karl, D. M. (1991). RACER: Research on Antarctic coastal ecosystem rates. *Deep Sea Research Part A. Oceanographic Research Papers*, *38*(8/9), R5–R7.

Kavanaugh, M. T., Abdala, F. N., Ducklow, H., Glover, D., Fraser, W., Martinson, D., . . . Doney, S. C. (2015). Effect of continental shelf canyons on phytoplankton biomass and community composition along the western Antarctic Peninsula. *Marine Ecology Progress Series*, *524*, 11–26.

Kemeny, P. C., Weigand, M. A., Zhang, R., Carter, B. R., Karsh, K. L., Fawcett, S. E., & Sigman, D. M. (2016). Enzyme-level interconversion of nitrate and nitrite in the fall mixed layer of the Antarctic Ocean. *Global Biogeochemical Cycles*, *30*, 1069–1085. https://doi.org/10.1002/2015GB005350

Kim, H., Doney, S. C., Iannuzzi, R. A., Meredith, M. P., Martinson, D. G., & Ducklow, H. W. (2016). Climate forcing for dynamics of dissolved inorganic nutrients at Palmer Station, Antarctica: An interdecadal (1993–2013) analysis. *Journal of Geophysical Research: Biogeosciences*, *121*, 2369–2389. https://doi.org/10.1002/2015JG003311

Klunder, M. B., Laan, P., Middag, R., De Baar, H. J. W., & van Ooijen, J. C. (2011). Dissolved Fe in the Southern Ocean (Atlantic sector). *Deep Sea Research Part II: Topical Studies in Oceanography*, *58*, 2678–2694.

Kropuenske, L. R., Mills, M. M., van Dijken, G. L., Alderkamp, A.-C., Berg, G. M., Robinson, D. H., . . . Arrigo, K. R. (2010). Strategies and rates of photoacclimation in two major Southern Ocean phytoplankton taxa: *Phaeocystis antarctica* (Haptophyta) and *Fragilariopsis cylindrus* (Bacillariophyceae). *Journal of Phycology*, *46*, 1138–1151. https://doi.org/10.1111/j.1529-8817.2010.00922.x

Langdon, C. (2010). Determination of dissolved oxygen in seawater by Winkler titration using the amperometric technique. In E. M. Hood, C. L. Sabine, & B. M. Sloyan (Eds.), *The GO-SHIP repeat hydrography manual: A collection of expert reports and guidelines*.

Lannuzel, D., Chever, F., van der Merwe, P. C., Janssens, J., Roukaerts, A., Cavagna, A.-J., . . . Meiners, K. M. (2016). Iron biogeochemistry in Antarctic pack ice during SIPEX-2. *Deep Sea Research Part II: Topical Studies in Oceanography*, *131*, 111–122.

Lannuzel, D., Grotti, M., Abelmoschi, M. L., & van der Merwe, P. (2015). Organic ligands control the concentrations of dissolved iron in Antarctic sea ice. *Marine Chemistry*, *174*, 120–130.

Mackey, M. D., Mackey, D. J., Higgins, H. W., & Wright, S. W. (1996). CHEMTAX—A program for estimating class abundances from chemical markers: Application to HPLC measurements of phytoplankton. *Marine Ecology Progress Series*, *144*, 265–283.

Marrari, M., Daly, K. L., & Hu, C. (2008). Spatial and temporal variability of SeaWiFS chlorophyll *a* distributions west of the Antarctic Peninsula: Implications for krill production. *Deep Sea Research Part II: Topical Studies in Oceanography*, *55*, 377–392.

Martinson, D. G., & McKee, D. C. (2012). Transport of warm Upper Circumpolar Deep Water onto the western Antarctic Peninsula continental shelf. *Ocean Science*, *8*, 433–442. https://doi.org/10.5194/os-8-433-2012

Martinson, D. G., Stammerjohn, S. E., Iannuzzi, R. A., Smith, R. C., & Vernet, M. (2008). Western Antarctic Peninsula physical oceanography and spatio-temporal variability. *Deep Sea Research Part II: Topical Studies in Oceanography*, *55*, 1964–1987.

Meredith, M. P., & King, J. C. (2005). Rapid climate change in the ocean west of the Antarctic Peninsula during the second half of the 20th century. *Geophysical Research Letters*, *32*, L19604. https://doi.org/10.1029/2005GL024042

Moffat, C., Owens, B., & Beardsley, R. C. (2009). On the characteristics of Circumpolar Deep Water intrusions to the west Antarctic Peninsula continental shelf. *Journal of Geophysical Research*, *114*, C05017. https://doi.org/10.1029/2008JC004955

Moline, M. A., Schofield, O., & Boucher, N. (1998). Photosynthetic parameters and empirical modelling of primary production: A case study on the Antarctic Peninsula shelf. *Antarctic Science*, *19*(1), 45–54.

Montes-Hugo, M., Doney, S. C., Ducklow, H. W., Frasr, W., Martinson, D., Stammerjohn, S., & Scofield, O. (2009). Recent changes in phytoplankton communities along the western Antarctic Peninsula associated with rapid regional climate change. *Science*, *323*, 1470–1473.

Moreau, S., Ferreyra, G. A., Mercier, B., Lemarchand, K., Lionard, M., Roy, S., . . . Demers, S. (2010). Variability of the microbial community in the western Antarctic Peninsula from late fall to spring during a low ice cover year. *Polar Biology*, *33*(12), 1599–1614.

Moreau, S., Mostajir, B., Belanger, S., Schloss, I. R., Vancoppenolle, M., Demers, S., & Ferrayra, G. A. (2015). Climate change enhances primary production in the western Antarctic Peninsula. *Global Change Biology*, *21*, 2191–2205. https://doi.org/10.1111/gcb.12878

Olson, R. J., Sosik, H. M., & Chekalyuk, A. M. (1999). Photosynthetic characteristics of marine phytoplankton from pump-during-probe fluorometry of individual cells at sea. *Cytometry*, *37*, 1–13.

O'Reilly, J. E., Maritorena, S., Mitchell, B. G., Siegel, D. A., Carder, K. L., Garver, S. A., . . . McClain, C. R. (1998). Ocean color chlorophyll algorithms for SeaWiFS. *Journal of Geophysical Research*, *103*, 24937–24953. https://doi.org/10.1029/98JC02160

O'Reilly, J. E., Maritorena, S., O'brien, M. C., Siegel, D., Toole, A., Menzies, D. C., . . . Culver, M. (2000). *SeaWiFS post launch calibration and validation analyses, Part 3* (NASA Tech. Memo. 2000–206892, Vol. 11, 49 pp.). Greenbelt, MD: NASA Goddard Space Flight Center.

Orsi, A. H., Whitworth, T., & Nowlin, W. D. (1995). On the meridional extent and fronts of the Antarctic Circumpolar Current. *Deep Sea Research Part I: Oceanographic Research Papers*, *42*, 641–673.

Perl, J. (2009). The SDSU (CHORS) method. In *The third SeaWiFS HPLC Analysis Round-Robin Experiment (SeaHARRE-3)* (NASA Tech. Memo 2009–215849, pp. 89–90). Greenbelt, MD: NASA Goddard Space Flight Center.

Planquette, H., Sanders, R. R., Statham, P. J., Morris, P. J., & Fones, G. R. (2011). Fluxes of particulate iron from the upper ocean around the Crozet Islands: A naturally iron-fertilized environment in the Southern Ocean. *Global Biogeochemical Cycles*, *25*, GB2011. https://doi.org/10.1029/2010GB003789

Planquette, H., Sherrell, R. M., Stammerjohn, S., & Field, P. M. (2013). Particulate iron delivery to the water column of the Amundsen Sea, Antarctica. *Marine Chemistry*, *153*, 15–30. https://doi.org/10.1016/j.marchem.2013.04.006

Raiswell, R. (2011). Iceberg-hosted nanoparticulate Fe in the Southern Ocean: Mineralogy, origin, dissolution kinetics and source of bioavailable Fe. *Deep Sea Research Part II: Topical Studies in Oceanography*, *58*(11–12), 1364–1375.

Raiswell, R., Benning, L. G., Tranter, M., & Tulaczyk, S. (2008). Bioavailable iron in the Southern Ocean: The significance of the iceberg conveyor belt. *Geochemical Transactions*, *9*, 7. https://doi.org/10.1186/1467-4866-9-7

Rodriguez, F., Varela, M., & Zapata, M. (2002). Phytoplankton assemblages in the Gerlache and Bransfield Straits (Antarctic Peninsula) determined by light microscopy and CHEMTAX analysis of HPLC pigment data. *Deep Sea Research Part II: Topical Studies in Oceanography*, *49*, 723–747.

Rozema, P. D., Venables, H. J., van de Poll, W. H., Clarke, A., Meredith, M. P., & Buma, A. G. J. (2017). Interannual variability in phytoplankton biomass and species composition in northern Marguerite Bay (West Antarctic Peninsula) is governed by both winter sea ice cover and summer stratification. *Limnology and Oceanography*, *62*, 235–252. https://doi.org/10.1002/lno.10391

Saba, G. K., Fraser, W. R., Saba, V. S., Iannuzzi, R. A., Coleman, K. E., Doney, S. C., . . . Schofield, O. M. (2014). Winter and spring controls on the summer food web of the coastal West Antarctic Peninsula. *Nature Communications*, *5*, 4318. https://doi.org/10.1038/ncomms5318

Sedwick, P. N., & DiTullio, G. R. (1997). Regulation of algal blooms in Antarctic shelf waters by the release of iron from melting sea ice. *Geophysical Research Letters*, *24*, 2515–2518.

Sedwick, P. N., Marsay, C. M., Aguilar-Islas, A. M., Lohan, M. C., Sohst, B. M., Long, M. C., . . . DiTullio, G. R. (2011). Early-season iron depletion in the Ross Sea polynya: Implications for iron dynamics on the Antarctic continental shelf. *Journal of Geophysical Research*, *116*, C12019. https://doi.org/10.1029/2010JC006553

Selz, V., Arrigo, K. R., Lowry, K. E., & Lewis, K. M. (2016). Ice algal contributions to pelagic production. *Eos Transactions of American Geophysical Union*, Abstract 90620.

Serebrennikova, Y. M., & Fanning, K. A. (2004). Nutrients in the Southern Ocean GLOBEC region: Variations, water circulation, and cycling. *Deep Sea Research Part II: Topical Studies in Oceanography*, *51*, 1981–2002.

Smith, R. C., Baker, K. S., Fraser, W. R., Hofmann, E. E., Karl, D. M., Klinck, J. M., . . . Vernet, M. (1995). The Palmer LTER: A Long-Term Ecological Research program at Palmer Station, Antarctica. *Oceanography*, *8*, 77–86.

Smith, R. C., Martinson, D. G., Stammerjohn, S. E., Iannuzzi, R. A., & Ireson, K. (2008). Bellingshausen and western Antarctic Peninsula region: Pigment biomass and sea ice spatial/temporal distributions and interannual variability. *Deep Sea Research Part II: Topical Studies in Oceanography*, *55*, 1949–1963. https://doi.org/10.1016/j.dsr2.2008.04.027

Smith, W. O., Jr., & Donaldson, K. (2015). Photosynthesis–irradiance responses in the Ross Sea, Antarctica: A meta-analysis. *Biogeosciences*, *12*, 3567–3577.

Smith, W. O., Jr., & Nelson, D. M. (1986). Importance of ice-edge phytoplankton production in the Southern Ocean. *BioScience*, *36*, 251–256.

Stammerjohn, S. E., Massom, R. A., Rind, D., & Martinson, D. G. (2012). Regions of rapid sea ice change: An inter-hemispheric seasonal comparison. *Geophysical Research Letters*, *39*, L06501. https://doi.org/10.1029/2012GL050874

Tagliabue, A., Sallee, J. B., Bowie, A. R., Levy, M., Swart, S., & Boyd, P. W. (2014). Surface-water iron supplies in the Southern Ocean sustained by deep winter mixing. *Nature Geoscience*, *7*(4), 314–320.

Thompson, A. F., & Youngs, M. K. (2013). Surface exchange between the Weddell and Scotia Seas. *Geophysical Research Letters*, *40*, 1–6. https://doi.org/10.1002/2013GL058114

Trimborn, S., Hoppe, C. J. M., Taylor, B. B., Bracher, A., & Hassler, C. (2015). Physiological characteristics of open ocean and coastal phytoplankton communities of western Antarctic Peninsula and Drake Passage waters. *Deep Sea Research Part I: Oceanographic Research Papers*, *98*, 115–124.

Turner, D. R., & Owens, N. J. P. (1995). A biogeochemical study in the Bellingshausen Sea: Overview of the STERNA 1992 expedition. *Deep Sea Research Part II: Topical Studies in Oceanography*, *42*(4–5), 907–932.

Turner, J., Maksym, T., Phillips, T., Marshall, G. J., & Meredith, M. P. (2012). The impact of changes in sea ice advance on the large winter warming on the western Antarctic Peninsula. *International Journal of Climatology*, *30*, 852–861. https://doi.org/10.1002/joc.3474

Van Heukelem, L., & Thomas, C. S. (2001). Computer-assisted high-performance liquid chromatography method development with applications to the isolation and analysis of phytoplankton pigments. *Journal of Chromatography A*, *910*, 31–49.

Van Leeuwe, M. A., Visser, R. J. W., & Stefels, J. (2014). The pigment composition of *Phaeocystis antarctica* (Haptophyceae) under various conditions of light, temperature, salinity, and iron. *Journal of Phycology*, *50*, 1070–1080.

Varela, M., Fernandez, E., & Serret, P. (2002). Size-fractionated phytoplankton biomass and primary production in the Gerlache and south Bransfield Straits (Antarctic Peninsula) in Austral summer 1995–1996. *Deep Sea Research Part II: Topical Studies in Oceanography*, *49*, 749–768.

Venables, H. J., Clarke, A., & Meredith, M. P. (2013). Wintertime controls on summer stratification and productivity at the western Antarctic Peninsula. *Limnology and Oceanography*, *58*, 1035–1047. https://doi.org/10.4319/lo.2013.58.3.1035

Vernet, M., Martinson, D., Iannuzzi, R., Stammerjohn, S., Kozlowski, W., Sines, K., . . . Garibotti, I. (2008). Primary production within the sea-ice zone west of the Antarctic Peninsula: I—Sea ice, summer mixed layer, and irradiance. *Deep Sea Research Part II: Topical Studies in Oceanography*, *55*, 2,068–2,085. https://doi.org/10.1016/j.dsr2.2008.05.021